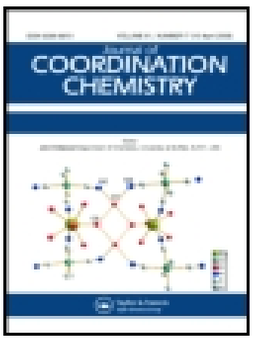

Journal of Coordination Chemistry

ISSN: (Print) (Online) Journal homepage: https://www.tandfonline.com/loi/gcoo20

Synthesis and biological activity of iron(II), iron(III), nickel(II), copper(II) and zinc(II) complexes of aliphatic hydroxamic acids

Ibrahima Sory Sow, Michel Gelbcke, Franck Meyer, Marie Vandeput, Mickael Marloye, Sergey Basov, Margriet J. Van Bael, Gilles Berger, Koen Robeyns, Sophie Hermans, Dong Yang, Véronique Fontaine & François Dufrasne

To cite this article: Ibrahima Sory Sow, Michel Gelbcke, Franck Meyer, Marie Vandeput, Mickael Marloye, Sergey Basov, Margriet J. Van Bael, Gilles Berger, Koen Robeyns, Sophie Hermans, Dong Yang, Véronique Fontaine & François Dufrasne (2023): Synthesis and biological activity of iron(II), iron(III), nickel(II), copper(II) and zinc(II) complexes of aliphatic hydroxamic acids, Journal of Coordination Chemistry, DOI: 10.1080/00958972.2023.2166407

To link to this article: https://doi.org/10.1080/00958972.2023.2166407

JOURNAL OF COORDINATION CHEMISTRY
https://doi.org/10.1080/00958972.2023.2166407

Synthesis and biological activity of iron(II), iron(III), nickel(II), copper(II) and zinc(II) complexes of aliphatic hydroxamic acids

Ibrahima Sory Sow[a], Michel Gelbcke[a], Franck Meyer[a], Marie Vandeput[b], Mickael Marloye[a], Sergey Basov[e], Margriet J. Van Bael[e], Gilles Berger[a], Koen Robeyns[c], Sophie Hermans[c], Dong Yang[d], Véronique Fontaine[a†] and François Dufrasne[a†]

[a]Microbiology, Bioorganic and Macromolecular Chemistry Unit, Faculty of Pharmacy, Université libre de Bruxelles (ULB), Brussels, Belgium; [b]Pharmacognosy, Bioanalysis and Drug Discovery Research Unit (RD3-PBM), Faculty of Pharmacy, Université libre de Bruxelles (ULB), Brussels, Belgium; [c]Institute of Condensed Matter and Nanosciences (IMCN), Molecular Chemistry, Materials and Catalysis (MOST), Université catholique de Louvain (UCLouvain), Louvain-la-Neuve, Belgium; [d]Clinical Laboratory, Shanxi Provincial People's Hospital, Affiliated of Shanxi Medical University, Taiyuan, China; [e]Quantum Solid State Physics, Department of Physics and Astronomy, KU Leuven, Leuven, Belgium

ABSTRACT

Aliphatic hydroxamic acids (HA) with varying numbers of carbon atoms, C_2, C_6, C_8, C_{10}, C_{12} and C_{17}, and corresponding Fe(II), Fe(III), Ni(II), Cu(II) and Zn(II) complexes have been synthesized and characterized by various methods, including structural determination by single crystal X-ray diffraction and theoretical calculations. The biological activities of HA and their complexes have been assessed on a panel of pathogens, including eight bacteria strains and one fungus. The C_{12} aliphatic HA displayed the lowest minimum inhibitory concentrations (MIC) towards several microbial strains and a selective antifungal activity. This antifungal selectivity was further improved considering the Ni(II), Cu(II) and Zn(II) complexes of C_{12} HA showed higher IC_{50} values, thus less impact on the SiHa human cell line viability. This work warrants further investigation to understand the underlying mechanism of action and potential biological applications of HA and the derived metal complexes.

ARTICLE HISTORY
Received 2 September 2022
Accepted 19 December 2022

KEYWORDS
Hydroxamic acids; metal complexes; antibacterial; antifungal; lipophilicity

CONTACT François Dufrasne Francois.Dufrasne@Ulb.be Microbiology, Bioorganic and Macromolecular Chemistry Unit, Faculty of Pharmacy, Université Libre de Bruxelles (ULB), Boulevard du Triomphe, 1050 Brussels, Belgium

Supplemental data for this article can be accessed online at https://doi.org/10.1080/00958972.2023.2166407.

†These authors contributed equally to this work.

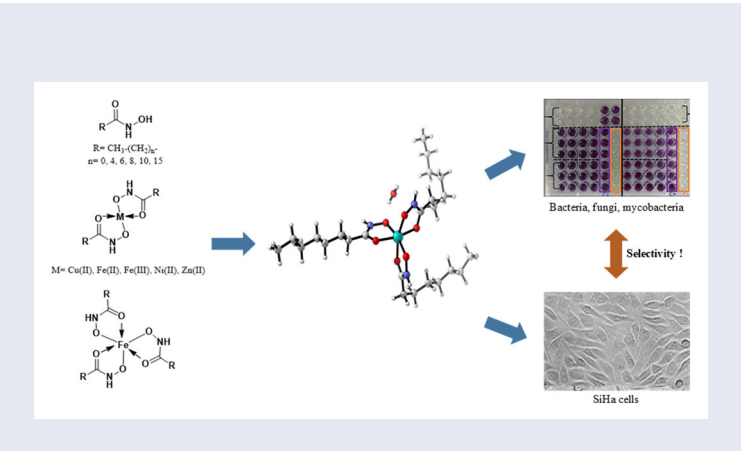

1. Introduction

The first hydroxamic acids (HA) were discovered by Lossen in 1869 (oxalohydroxamic: HONH-CO-CO-NHOH), but this class of organic compounds was only thoroughly studied from the nineteen eighties [1]. HA are among some of the most well studied compounds due to their significance in so many different applications in modern society [2].

HA have various applications in biology, industry and medicine as growth factors, food additives, anticancer agents, pigments and chelating agents [3, 4]. Some compounds have been reported with antimicrobial properties [4], especially against bacteria and fungi [5, 6]. The 3,5-dinitrobenzohydroxamic acid and its Zn(II) complex exhibit antibacterial activities against *Streptococcus pneumoniae* but not against *Staphylococcus aureus*, *Escherichia coli* and *Pseudomonas aeruginosa* [7]. Complexation of HA to metals resulted in increased antimicrobial activity [7–9]. Aceto- and propiono-HA complexed to Ni(II) along with valero- and isovalero derivatives complexed with Fe(III), Mn(II), Al(III) and Zn(II) were also reported to have antibacterial properties [10, 11]. *N*-Caproyl benzohydroxamic acids and their Cu(II) and Ni(II) complexes displayed bacteriostatic activities against *S. aureus*, *E. coli* and antifungal activities against *Aspergillus niger* and *Aspergillus flavus* [8]. Other examples comprise metal complexes from pyrimidine-derived HA showing significant antibacterial and antifungal growth inhibition [9]. Finally, *N*-2′-phenylaceto-, 2,2′-diphenylaceto-, 2-phenylaceto-HA and their Cu(II), Ni(II) and Co(II) complexes were also reported with antifungal activities towards *Alternaria alternata*, *Fusarium oxysporum* and *A. flavus* [12]. A series of aromatic HA, with the general formula PhNOHCOR (R = H, $C_{11}H_{23}$, $C_{13}H_{27}$), and their Cu(II) complexes have strong antifungal activities against several fungi (*Candida parapsilosis*, *Candida albicans* and *Aspergillus fumigatus*) [13].

HA also display antimycobacterial activity against *Mycobacterium tuberculosis* [14] and *Mycobacterium smegmatis* [15]. They are powerful inhibitors of enzymes such as hydrolase [16], urease [17], thermolysin [18], aminopeptidase [19, 20], tyrosinase [21] and matrix metalloproteinases (MMP) [22] by chelation of metal co-factors, in particular Fe(III) and Zn(II) [23, 24]. Desferrioxamine is used clinically to treat metal poisoning,

highlighting the strong chelating properties of the HA group [24, 25]. Systematic biological evaluation of large series of such compounds however remains scarce and the variability of methods used in previous work renders global interpretation of the results rather tedious. Therefore, a comparative study of the biological activity of HA with various alkyl chain lengths in combination with various metal centers could help draw conclusive results.

Numerous complexes with HA are reported such as: Cu(II) complexes of aceto- and octano-HA [26], tris-chelate complex of Fe(III) with aceto-HA [27] and similar complex with heptano- and octano-HA [28], Fe(II), Fe(III), Co(II), Ni(II), Cu(II) and Zn(II) complexes of aceto-, propiono-, benzo-, *N*-methyl-, stearo- and *N*-phenylbenzo-HA and references cited therein were prepared and characterized [29–31]. However, a single experimental study comprising the relationship between the biological activity and the structure of representative aliphatic HA and their complexes has not been done yet.

The aim of the present study is to evaluate the physico-chemical and biological properties of aliphatic hydroxamic acids (HA) with various chain lengths (C_2, C_6, C_8, C_{10}, C_{12} and C_{17}) and their Fe(II), Fe(III), Ni(II), Cu(II) and Zn(II) complexes. HA with the general formula RCONHOH and the derived metal complexes $(RCONHO)_2Fe$, $[(RCONHO)_2Fe]^+[Cl]^-$, $(RCONHO)_3Fe$, $(RCONHO)_2Ni$, $(RCONHO)_2Cu$ and $(RCONHO)_2Zn$ (with R = $-CH_3$, $-(CH_2)_4CH_3$, $-(CH_2)_6CH_3$, $-(CH_2)_8CH_3$, $-(CH_2)_{10}CH_3$ and $-(CH_2)_{15}CH_3$) have thus been synthesized and characterized by spectroscopic methods and cyclic voltammetry. Their stability and partition coefficient have also been determined. Subsequently, antimicrobial activities were investigated on eukaryotic (unicellular yeast) and prokaryotic (bacteria) cells, along with mycobacteria. Gram negative and Gram positive bacteria have been used to highlight the influence of the bacterial cell wall on the activity.

2. Materials and methods

2.1. Materials

2.1.1. Chemicals materials

Anhydrous $FeCl_2$, methyl-, hexyl-, decyl-, dodecyl-methanoate and 3-(4,5-dimethylthiazol-2yl)-2,5-diphenyl tetrazolium bromide (MTT) were obtained from Acros Organics (New Jersey, USA). Ethyl acetate (AcOEt), NaOH, dichloromethane (DCM), dimethyl sulfoxide (DMSO) and oxalic acid ($H_2C_2O_4{\cdot}2H_2O$) were purchased from Chem-Lab NV (Leuven, Belgium). KOH pellets, acetic acid, DMSO-d_6, $CDCl_3$, nitric acid, silver nitrate and ammonia were obtained from Avantor (Leuven, Belgium). Hydroxylammonium chloride, butanol, $ZnCl_2$, $CuCl_2{\cdot}2H_2O$, $NiCl_2{\cdot}6H_2O$, dodecanoic acid, TLC silica GF_{254} chromatographic plates, P_2O_5, iodine, phosphomolybdic acid and rifampicin were purchased from Merck (Darmstadt, Germany). *N*-Methylmorpholine, methanol, octanol, heptadecanoic acid and vancomycin were obtained from Sigma-Aldrich (St. Louis, MO, USA). Ethyl choroformate, acetic anhydride, acetyl-, hexanoyl- and octanoyl-chloride, $MgSO_4{\cdot}7H_2O$ and hydranal coulomat AG (reagent for coulometric KF titration) were purchased from Fluka (Buchs, Switzerland). Anhydrous $FeCl_3$, hexanoic-, octanoic- and decanoic- acid were obtained from Alfa Aesar (Kandel, Germany). Cetrimide was purchased from Cetavlon of ICI-Pharma (Destelbergen, Belgium) and KCl was obtained from Panreac (Barcelona, Spain).

2.1.2. Biologicals materials

Mueller Hinton Broth (MHB) and Tryptic Soy Agar (TSA) were purchased from Sigma-Aldrich (Saint Louis, USA). Bacterial methicillin-sensitive *Staphylococcus aureus* (MSSA, LMG 8064), methicillin-resistant *Staphylococcus aureus* (MRSA, LMG 15975), *Corynebacterium glutamicum* (LMG 19741), *Bacillus subtilis* (DSM 618), *Escherichia coli* (LMG 8223), *Pseudomonas aeruginosa* (LMG 6395), *Klebsiella pneumoniae* (LMG 20218) and fungal *Candida albicans* (IHEM 9559) were purchased from Belgian Coordinated Collection of Microorganisms (BCCM), University of Gent. *Mycobacterium smegmatis* (CIP 7326) was obtained from the Pasteur Institute in Paris. The SiHa cell line was obtained from the American Type Culture Collection (ATCC).

2.2. Methods

2.2.1. Chemical and physical methods

All the syntheses of HA were followed by TLC on GF_{254} silica chromatographic plates. The revelations were made by a UV lamp (254 nm), iodine or a solution of phosphomolybdic acid 10% in ethanol. The solvents were evaporated using a rotary evaporator.

^{1}H and ^{13}C NMR spectra were recorded with a JEOL JNM-ECZ 400 R/S3 type NMR spectrometer (Tokyo, Japan), respectively, at 400 MHz and 100 MHz by dissolving about 10 mg of product in 500 µL of deuterated solvents (DMSO-d_6 or $CDCl_3$). The chemical shifts are given in parts per million (ppm) using the residual solvent peak as reference (2.50 and 7.26 ppm for DMSO-d_6 and $CDCl_3$, respectively), and the coupling constants are expressed in Hertz (Hz). The IR spectra were recorded on a Perkin Elmer FT-IR-MIR/NIR (Beaconsfield, UK) spectrophotometer equipped with an ATR Diamond KRS-51 module using 2-3 mg of each product within a wavenumber range 400-4000 cm^{-1}. Raman spectra were taken with a Bruker FT-Raman spectrometer RFS 100/S (Massachusetts, USA) equipped with a Michelson interferometer for Fourier transform. The source is a near-IR Nd^{3+}: YAG laser at 1064 nm wavelength, while the Ge detector is cooled with liquid nitrogen. The Raman spectra were recorded with power ranging from 50 to 250 mW depending on the nature of the sample, as a compromise between best quality spectra and decomposition of the sample under the laser beam. The highest possible power was used for each sample by increasing gradually the power within this range during each recording. The solid samples were introduced into the cavity of a small metallic sample holder using a small funnel and pestle. The resolution was fixed at a value of 4 cm^{-1}, and for each sample 48 scans were recorded in the 0 to 4000 cm^{-1} range. Elemental sulfur is used as a reference to verify all experimental parameters before analyzing research samples. The UV spectra were recorded with a spectrophotometer Shimadzu UV-1800 (Kyoto, Japan). 5 mM solutions were prepared by dissolving the appropriate amount of product in MeOH. Then 100 µL of this solution were taken and diluted to 5 mL with MeOH (final solution at 100 µM). With Cu(II), Zn(II) and Ni(II) complexes, a second dilution was carried out to have a final concentration of 50 µM. The mass spectra (MS) were obtained with a Q-TOF-6520 spectrometer from Agilent (Santa Clara-California, USA). The MS of complexes are given with a *m/z* range from 100 to 1700 in positive mode. MS were obtained by dissolving

1–1.5 mg of complexes in 1 mL of MeOH, then diluted 1/100 in a mixture of 0.2% formic acid in water – MeOH (2: 8).

Electron paramagnetic resonance (EPR) spectra of some Fe(III) and Cu(II) complexes and some HA were recorded on a Bruker Magnettech ESR5000 CW benchtop spectrometer operating at 9.4 GHz (X-band). Spectra of the Fe(III) complexes were recorded at 93.15 K and, for HA, at room temperature. EPR measurements of the Cu(II) complexes were not recorded ($C \approx 0.3$ mol/L, insufficient solubility in $CHCl_3$ for the EPR analysis). For these measurements, 20 μL of a freshly prepared solution of the HA ($C \approx 1$ mol/L) or Fe(III) complexes in CH_3OH ($C \approx 0.1$ mol/L) was filled in a 3 mm EPR tube.

Elemental analyses have been determined on a Perkin Elmer 2400 elemental analyzer equipped with a sixty (60) sample autosampler. The results processing system were managed by EA 2400 data manager software. Melting points (uncorrected) were determined on a Büchi B-545. Stability of complexes in water was assessed by UV spectroscopy in the range 200-800 nm [32]. Methanolic solutions of complexes (20 mM) were further diluted to 1 mM with the same solvent. Subsequently, MilliQ water was added to obtain 50 and 100 μM solutions (5 and 10% MeOH). The UV spectra were recorded on a spectrophotometer Cary 60 (Agilent), including one spectrum each 5 min during 30 min and one spectrum each 30 min during 24 h.

The amount of water in the complexes was determined according to the Karl Fischer method with a 756 KF Coulometer from Metrohm (Antwerpen, Belgium). 25.0 mg of complexes were weighted into an Eppendorf tube and dissolved in 500 μL of MeOH. Then, 200 μL of this solution was injected through the septum of the device via a syringe. Two reference salts were used to validate this experiment ($H_2C_2O_4{\cdot}2H_2O$, $MgSO_4{\cdot}7H_2O$). All experiments were repeated twice for each sample. A blank analysis (methanol) was done for each sample. The complexes were kept 24 h in a dry atmosphere before analysis to avoid hygroscopic water.

X-ray diffraction data were collected on a MAR345 image plate detector (Hamburg, Germany) using Mo Kα radiation generated by a Rigaku Ultra X18S rotating anode (Tokyo, Japan). Crystals for structure determination were obtained for the Fe(III) complexes, giving red-orange plate like crystals after evaporation of a MeOH/DCM solution (1: 9). The collected images were integrated and reduced by CrysAlis^{PRO} and the implemented absorption correction was applied. Structure was solved by SHELXT and refined by full-matrix least squares against F^2 using SHELXL 2014/7. Quantum mechanical methods for density functional theory (DFT) calculations have been achieved using Orca 4.2.1 [33], performed in the gas phase. Geometries were fully optimized with the triple-ζ quality, low-cost method B97-3c from Grimme and co-workers [34]. Potential energy surface minima found upon optimization were confirmed by frequency calculations and free energies were corrected to account for the zero-point energy. Optimized geometries were verified as minima (*i.e.* no imaginary frequencies).

The cyclic voltammetry (CV) experiments were performed with an Epsilon potentiostat BASi (west Lafayette, USA) connected to a carbon screen-printed electrode (DRP-110) from Dropsens (Asturias, Spain). The cSPE constituted of a miniaturized cell with 3 electrodes all in one includes a carbon working electrode, a carbon counter electrode and a silver pseudo reference electrode. The software Epsilon-EC-version 1.50.69_XP was used for instrument control. For CV experiments, stock solutions of the

samples (HA, salts and complexes) were prepared in MeOH to obtain a concentration of 10 mM. These solutions were subsequently diluted with a 1 M KCl aqueous solution as support electrolyte and with 5% MeOH (in order to avoid any risk of reprecipitation of samples in aqueous solution) to a final concentration of 100 μM. A volume of 50 μL of this solution was carefully deposited on all surfaces of the miniaturized cSPE. Between each CV measurement, a new cSPE was used to avoid the so-called "memory" effects and solutions were deoxygenated with nitrogen for at least 5 min before each measurement to ensure no interference with dissolved oxygen. The potentials ranged from either −0.2 V or −0.4 V to +1.2 V. Then, the scanning was reversed toward the initial value. The cyclic voltammograms were carried out in one scan and multiple scans (10 cycles) at a scanning rate of 50 mV/s.

Partition coefficients (logP) were determined for all synthesized compounds [32]. 10 mg of each compound were partitioned between 1 mL of n-octanol and 1 mL of water. After stirring for 1 h, 25 μL were taken in each phase and then diluted to 2.0 mL with the corresponding solvent. The absorbances of the different solutions were measured in the organic and aqueous phases by UV spectroscopy (ℰ in both solvents were not significantly different). The spectra were recorded in the range 200-700 nm using a Shimadzu UV-1800 instrument. For each compound three measurements were performed. The concentrations of compounds dissolved in water (C_{water}) and octanol ($C_{octanol}$) were calculated by applying the Beer-Lambert law (Eq. 1). The logP was calculated for each experiment (Eq. 2). The average logP was obtained from three independent experiments.

$$A = \varepsilon \times l \times C \tag{1}$$

$$LogP = \log \frac{C_{octanol}}{C_{water}} \tag{2}$$

A: absorbance, ℰ: molar absorption coefficient (L/mol·cm), l: optical path length (cm) and C: concentration (mol/L).

Magnetic measurements were carried out in a superconducting quantum interference device magnetometer (Quantum Design SQUID VSM MPMS3). Hysteresis loops were measured on dried samples in plastic capsules at 300 K with a maximum field of 10 kOe. The magnetization was normalized to the powder mass determined by subtracting the weight of the capsule from the total weight of the sample. A reference measurement using a Pd reference sample was conducted to quantify the remanent moment from the superconducting magnet, which allowed correction of the field values in the hysteresis loops. A linear diamagnetic background contribution from the sample holder was subtracted from the magnetic moment data of the complexes (Figure S19). The effective magnetic moment (μ_{eff}) which gives the effective number of μ_B per molecule was calculated using the following equation [35]:

$$\mu_{eff} = 797.8 \sqrt{\chi_M \times T} \tag{3}$$

χ_M: molar magnetic susceptibility = mass susceptibility × molar mass, T: temperature (300 K) and μB is the Bohr magneton.

Here χ_M is the value of the molar magnetic susceptibility in units of $m^3\ mol^{-1}$ which equals the mass susceptibility multiplied by the molar mass, T is the value of the temperature in units of K, and μB is the Bohr magneton.

After measuring the electrical conductivity of the compounds using the TetraCon® 325 conductivity meter, the molar conductance was calculated (Eq. 4). Stock solutions at different concentrations were prepared in 2 mL of MeOH (C_0) and then diluted 20 times in the same solvent. MeOH (blank) was used as reference.

$$MC = \frac{EC}{C_1} \tag{4}$$

C_0: initial concentration (mol·cm^{-3}), C_1: final concentration studied (C_0 diluted 20 times), EC: electric conductivity ((Ω^{-1}cm^{-1}), MC: molar conductance ((Ω^{-1}cm^{2}mol^{-1}).

2.2.2. Biological methods

2.2.2.1. Antimicrobial assay. The antibacterial, antimycobacterial and antifungal activity assays were performed using the microdilution method [36]. The stock solutions were at 200 mM in DMSO for HA, Fe(II/III) complexes (HAnFe2, HAnFeCl and HAnFe3) and metal chloride ($FeCl_2$, $FeCl_3$, $CuCl_2$, $ZnCl_2$ and $NiCl_2$) and in MeOH for Cu(II), Zn(II) and Ni(II) complexes (HAnCu2, HAnZn2 and HAnNi2). Volumes of 5 μL and/or 25 μL of stock solution were added to the MHB to a final volume of 1000 μL to obtain a final concentration of 1 mM and/or 5 mM (solutions containing 1% and/or 5% of DMSO or MeOH, v/v). The aqueous stock solutions of antibiotics/antiseptic were 69 mM (100 mg/mL), 0.6 mM (0.2 mg/mL) and 12 mM (10 mg/mL) for vancomycin, cetrimide and rifampicin, respectively. These solutions were subsequently diluted in MHB to achieve a final concentration of 7 μM (10 μg/mL), 6 μM (2 μg/mL) and 12 μM (10 μg/mL), respectively. These samples were subsequently diluted within 2-fold dilution series in 96-well plates giving a final volume of 100 μL. Compound concentrations were rounded to the nearest hundredth.

The precultures of bacteria, mycobacteria and fungi were diluted to obtain a turbidity of 0.5 McFarland corresponding to approximately 1.5×10^8 colony forming units (CFU) per mL measured with a nephelometer. Then the diluted microbial suspensions were further diluted 100 times to achieve 1.5×10^6 CFU/mL and 100 μL of bacteria/mycobacteria/fungi were inoculated into 96-well plates containing 100 μL of diluted HA, complexes, salts or antibiotics/antiseptic. The plates were incubated at 37 °C for 24 h (bacteria), at 30 °C for 48 h (mycobacteria), at 30 °C (*B. subtilis*) for 48 h, and at 22 °C (*C. albicans*) for 48 h.

The next day, 30 μL of MTT dissolved in MilliQ water (80% m/v) were added to the plate and incubated for 30 to 60 min. The minimum inhibitory concentrations (MIC) were obtained by visual observation and corresponded to the lowest concentration of drug/antibiotic/antiseptic able to inhibit 100% microorganism growth compared to control wells without drugs. In addition, the minimum bactericidal/minimum fungicidal concentration (MBC/MFC) were determined by transferring well samples with drug concentrations $\geq$ MIC on TSA plates. MBC/MFC represented the lowest concentration of tested drug/antibiotic/antiseptic required to kill 99.9% of microorganisms, recorded by visual analysis on the second or third growth day, when untreated bacteria were giving colonies [37]. If the MBC/MIC or MFC/MIC ratios were 1 or 2, the effect was considered as bactericidal/fungicidal. In contrast, if this ratio was equal to 4 or 16, the effect was defined as bacteriostatic/fungistatic [38].

2.2.2.2. Cytotoxicity assay. The cytotoxicity assays on SiHa cells were carried out as previously described [39]. For 24 h, the SiHa cells were grown in Dulbeccos's Modified Eagle Medium (DMEM) with 10% (v/v) fetal bovine serum (FBS) at 37 °C with 5% CO_2. The cells were diluted to a concentration of 7.6×10^5 cells/mL and further grown for another 24 h at 37 °C in humidified atmosphere containing 5% CO_2 in 96-well plates (100 µL/well). The drug stock solutions were 20 mM in DMSO (HA6Fe3, HA8FeCl, HA8Fe3, HA10FeCl, HA10Fe3, HA12, HA12Fe2, HA12FeCl, HA12Fe3) or in MeOH (HA12Cu2, HA12Zn2, HA12Ni2) and diluted hundred times in DMEM to a final concentration of 200 µM (0.2% solutions of DMSO/MeOH). These samples were subsequently diluted in DMEM within 2-fold dilution series in 96-well plates giving a final volume of 100 µL. A positive control was set up without drugs. The plates were incubated at 37 °C in a humidified atmosphere containing 5% CO_2 for 72 h. Then, 20 µL MTT (0.5 mg/mL in RPMI-1640) were added to each well and after 4 h incubation at 37 °C with 5% CO_2, the supernatant was removed and cells were washed with phosphate buffered saline (PBS) several times. Subsequently, 100 µL DMSO were added to each well and shaken for 10 min. The absorbances at 570 nm (the maximum formazan absorbance wavelength) and 630 nm (the background noise wavelength) were recorded using a spectrophotometer (Synergy HT, Bio-Tek). The average of the relative activity was calculated from the difference of the absorbances obtained at 570 and 630 nm for each test. The raw data were transferred to a Microsoft Excel sheet and analyzed. The percentage inhibition of cells using Eq. (5) and the cell viability was calculated according to Eq. (6) [40, 41].

$$\text{Inhibition}(\%) = \frac{A_0 - A_1}{A_0} \times 100 \tag{5}$$

$$\text{Viability}(\%) = \frac{A_1}{A_0} \times 100 \tag{6}$$

A_0: absorbance of the cells without drug (the positive control) and A_1: relative absorbance of the cells with drug.

The 50% inhibitory concentration (IC_{50}) values were also measured. The reduction of cell viability at each concentration was plotted as a dose response curve. The IC_{50} values were calculated from the dose response curves by nonlinear regression to fit data to the cell viability (y) – decimal logarithm of the concentration (logC) [42]. The selectivity index (SI) was calculated by Eq. (7). A SI greater than or equal to 10 indicates that the test compound can be applied at a concentration that is ten-fold higher than the MIC value without exhibiting cytotoxicity [43].

$$SI = \frac{IC_{50}}{MIC} \tag{7}$$

2.2.2.3. Statistical analysis. The antimicrobial results (MIC) were analyzed using t-test (Excel ®) at the statistical significance level of $p \leq 0.05$. Two sets of data were used for this purpose (bilateral distribution). The first series concerns the MIC results obtained with HA and complexes and the second concerns the MIC obtained with vancomycin, cetrimide and rifampicin from the three independent experiments carried out (see SI).

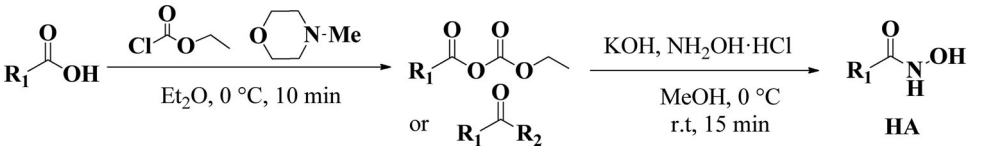

Scheme 1. Synthetic routes to the HA from carboxylic acids, esters or acid chlorides. R_1 = -CH_3, -$(CH_2)_4CH_3$, -$(CH_2)_6CH_3$, -$(CH_2)_8CH_3$, -$(CH_2)_{10}CH_3$, and -$(CH_2)_{15}CH_3$; R_2 = -OCH_3 and Cl.

Table 1. Formulas and codes of the synthesized HA and complexes.

	Codes of HA and complexes with carbon chains C_2, C_6, C_8, C_{10}, C_{12} and C_{17}					
Formulas	C_2	C_6	C_8	C_{10}	C_{12}	C_{17}
RCONHOH	HA2	HA6	HA8	HA10	HA12	HA17
$(RCONHO)_2Fe$	HA2Fe2	HA6Fe2	HA8Fe2	HA10Fe2	HA12Fe2	HA17Fe2
$[(RCONHO)_2Fe]^+$ $[Cl]^-$	HA2FeCl	HA6FeCl	HA8FeCl	HA10FeCl	HA12FeCl	HA17FeCl
$(RCONHO)_3Fe$	HA2Fe3	HA6Fe3	HA8Fe3	HA10Fe3	HA12Fe3	HA17Fe3
$(RCONHO)_2Cu$	HA2Cu2	HA6Cu2	HA8Cu2	HA10Cu2	HA12Cu2	HA17Cu2
$(RCONHO)_2Zn$	HA2Zn2	HA6Zn2	HA8Zn2	HA10Zn2	HA12Zn2	HA17Zn2
$(RCONHO)_2Ni$	HA2Ni2	HA6Ni2	HA8Ni2	HA10Ni2	HA12Ni2	HA17Ni2

R = -CH_3, -$(CH_2)_4CH_3$, -$(CH_2)_6CH_3$, -$(CH_2)_8CH_3$, -$(CH_2)_{10}CH_3$ and -$(CH_2)_{15}CH_3$.

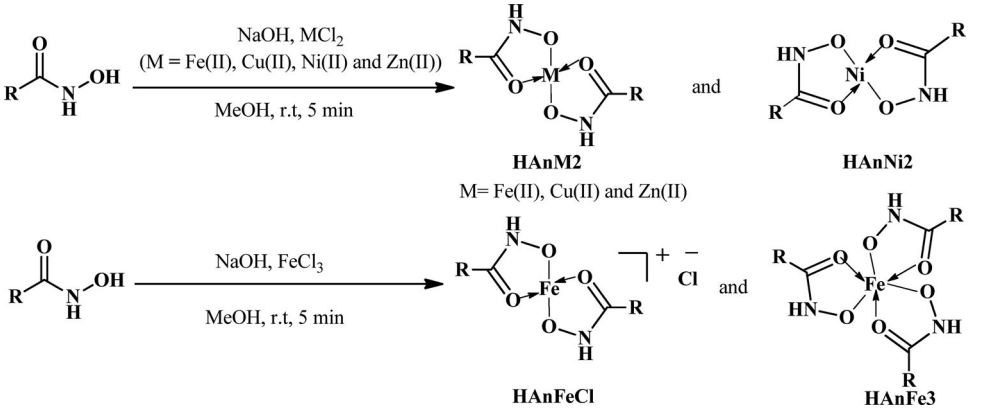

Scheme 2. Synthetic routes to the metal complexes: HAnM2, HAnNi2, HAnFeCl and HAnFe3. n = 2, 6, 8, 10, 12 and 17 (R = -CH_3, -$(CH_2)_4CH_3$, -$(CH_2)_6CH_3$, -$(CH_2)_8CH_3$, -$(CH_2)_{10}CH_3$, and -$(CH_2)_{15}CH_3$, respectively).

3. Results

3.1. Synthesis

HA were synthesized either from carboxylic acids through activation by ethyl chloroformate or starting from esters or acid chlorides (1 equivalent) and reacting them with a hydroxylamine solution (Scheme 1). This synthetic method was inspired by previously reported protocols [44, 45].

The metal complexes HAnFe2, HAnFeCl, HAnFe3, HAnCu2, HAnZn2 and HAnNi2 (with n = 2, 6, 8, 10, 12 and 17) were obtained from methanolic solutions of the HA and inorganic salts: $FeCl_2$, $FeCl_3$, $CuCl_2{\cdot}2H_2O$, $ZnCl_2$ or $NiCl_2{\cdot}6H_2O$, respectively (see Table 1). Precipitates were obtained after addition of water. This method, adapted from several published procedures [46–48], gave the di-hydroxamato Fe(II), Cu(II),

Zn(II), Ni(II), di-hydroxamato chloride Fe(III) or tri-hydroxamato Fe(III) complexes (Scheme 2). Minor impurities remained in some compounds, as evidenced by elemental analysis (see Appendix B). However, a further purification step of selected complexes (see section 3.3.1. Antimicrobial effect) led to identical physico-chemical data.

3.2. Characterization data

The HA and their complexes were obtained in 60 to 86% yields (Figure S1) and characterized by FTIR, stability analyses, mass spectrometry, Raman, UV-Vis, $^{1}H/^{13}C$ NMR and EPR spectroscopic methods (Figures S2–S14). KF titration was used for water determination and CV for redox properties. Single crystals suitable for X-ray structure determination were only obtained for HA8Fe3. Melting points and elemental analyses are given in table S1 and chloride ions of Fe(III) complexes (HAnFeCl) were identified by precipitation of AgCl using $AgNO_3$ (Figure S15).

3.2.1. IR spectroscopy

The IR absorbances are shown in Table S2 (for spectra, see Figure S2). Bands of medium (m) and sharp (sh) intensity in the 3200 cm^{-1} region can be attributed to the stretching vibration of the O-H group. Medium to strong (s) bands that are specific of the N-H bond stretch are found around 2800 cm^{-1}. The strong bands at 1650 cm^{-1} are characteristic of the carbonyl group (C = O), while bands at 1560, 1470 and 1370 cm^{-1} can be assigned to elongation of the C-N bond.

The main spectral change in the complexes is the disappearance of the hydroxyl ν(OH) peak due to the replacement of the hydrogen atom by transition metal ions. IR spectra of the complexes HAnFe2, HAnFeCl and HAnFe3 showed absorption bands between 3160-3200 cm^{-1}. The bands at 1520 and 1595 cm^{-1} arise from the carbonyl group (C = O), while signals between 1320 and 1470 cm^{-1} come from the C-N bond. Finally, strong absorption bands observed in the low energy region at 520 and 438 cm^{-1} are attributed to the Fe-O stretching vibrations. The Cu(II), Zn(II) and Ni(II) complexes displayed characteristic bands located between 3190-3250 cm^{-1}. Unlike HAnFe2, HAnFeCl and HAnFe3 complexes, HAnCu2, HAnZn2 and HAnNi2 complexes show narrower stretching bands. The medium to strong intensity resonances around 2900 cm^{-1} arise from stretching of the N-H bond. The strong bands at 1539 and 1599 cm^{-1} are attributed to the carbonyl group (C = O). Between 1340 and 1470 cm^{-1} are found the frequencies from the C-N bond. Finally, medium to strong absorption bands at 550-490 cm^{-1} could be attributed to the Cu-O, Zn-O and Ni-O bonds. Raman spectra for all HA, HAnFe2, HAnFeCl, HAnFe3 and HAnZn2 complexes are shown in Figure S3.

3.2.2. UV-Vis spectroscopy

Comparison of the UV-Vis spectra from HA10Fe2, HA10FeCl and HA10Fe3 helped attributing the HA-metal stoichiometry (Figure 1A). The maximum of absorption for the solutions of these complexes is found at 425 nm, with different extinction coefficients depending on the oxidation state (Fe(II) or Fe(III)). The highest $\mathcal{E}$ is observed for HA10Fe3 ($\mathcal{E} = 2350\ M^{-1}\ cm^{-1}$), followed by that of HA10Fe2 ($\mathcal{E} = 1600\ M^{-1}\ cm^{-1}$), HA10FeCl having the lowest one ($680\ M^{-1}\ cm^{-1}$). The UV-Vis spectra of HA8Cu2, HA8Zn2 and HA8Ni2

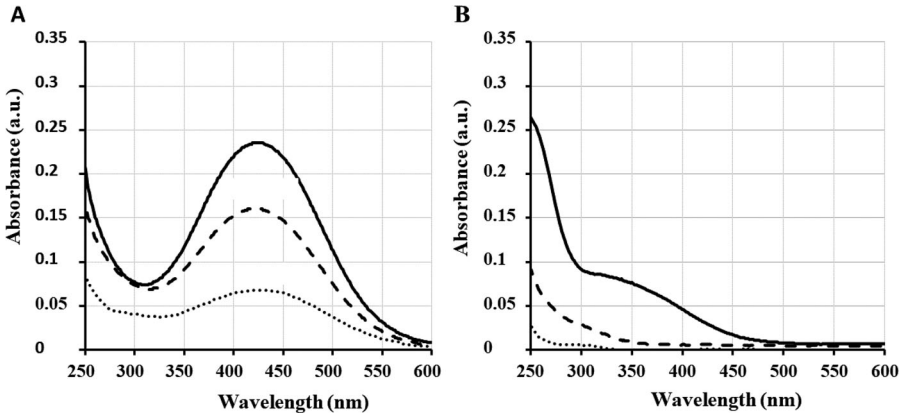

Figure 1. UV-Vis spectra of HA10-Fe complexes in MeOH. HA10Fe2 (dashed), HA10FeCl (dotted), HA10Fe3 (full line) at 100 μM (A); UV-Vis spectra of the HA8-Cu/Ni/Zn complexes in MeOH. HA8Cu2 (full line), HA8Ni2 (dashed) and HA8Zn2 (dotted) at 50 μM (B).

(Figure 1B) show maxima of absorption around 250 nm with the highest ε obtained for the HA8Cu2 (7300 $M^{-1}\,cm^{-1}$), followed by the HA8Ni2 ($\varepsilon = 2280\,M^{-1}\,cm^{-1}$) and HA8Zn2 ($\varepsilon = 1040\,M^{-1}\,cm^{-1}$). Similar results were observed under the same conditions with the other complexes having the same type of coordination metal (Figure S4).

3.2.3. EPR spectroscopy

EPR spectra have been recorded for Fe(III) complexes in MeOH solution at 0.1 mol/L (HA6Fe3, HA8Fe3 and HA12Fe3). A broad signal is observed under the magnetic field strength 165 mT for the three complexes (Figure S13). As expected, compounds HA6, HA10 and HA12 do not show any signal in EPR (data not shown).

3.2.4. Karl Fischer titrations

The water content was determined by the KF coulometric method. All HA2-containing complexes HA2Fe2, HA2FeCl, HA2Fe3, HA2Cu2, HA2Zn2 and HA2Ni2 were all obtained without water molecules. The Fe(II/III) complexes with an aliphatic chain longer than C_2 comprised one water molecule. Their Zn(II) and Ni(II) homologues crystallized with 0.5 water molecule. No water molecules were found in Cu(II) complexes. Therefore, the water content in these compounds varied depending on the type of metal but also the synthetic pathway.

3.2.5. Cyclic voltammetry

Cyclic voltammetry (CV) curves of all HA show an irreversible anodic peak (Ea_1). For short alkyl chain HA (HA2, HA6, HA8), this oxidation peak is observed at +1.0 V, +0.9 V and +0.8 V, respectively (Figure 2A). For HA with longer alkyl chain (HA10, HA12 and HA17), this irreversible anodic peak (Ea_1) is observed at lower potential (+0.6-0.7 V, Figure 2B–D).

The oxidation peak tends to disappear when multiple scanning is carried out. During the reverse scan, a reversible redox couple appeared with a broad reduction peak (Ec_2) starting at −0.2 V and a broad oxidation peak (Ea_2) at +0.4 V. These were also observed when starting at 0.0 V towards negative values, indicating a reduction. It

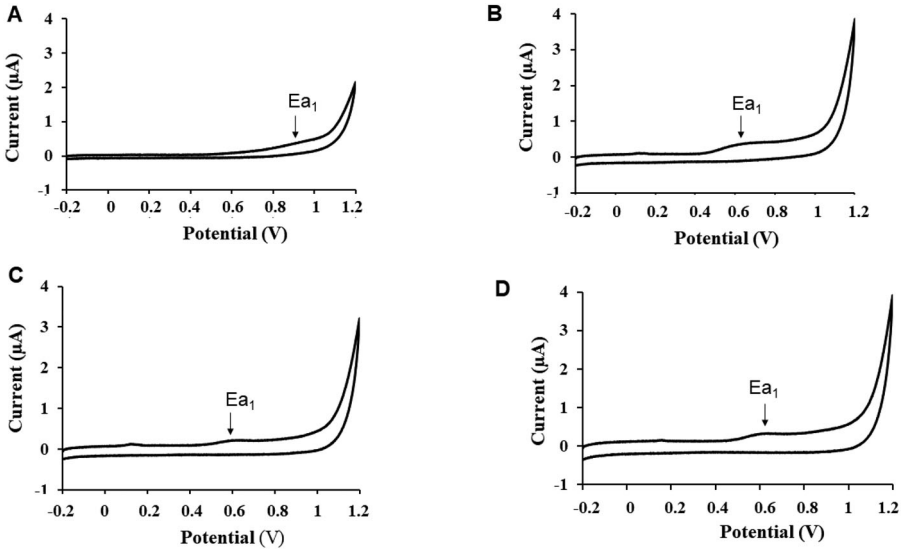

Figure 2. CV of HA6 (A), HA10 (B), HA12 (C) and HA17 (D) at 100 µM in KCl 1 M with 5% MeOH obtained at scan rate of 50 mV/s (1 cycle) with potentials in the range of -0.2 to +1.2 V and reverse scans.

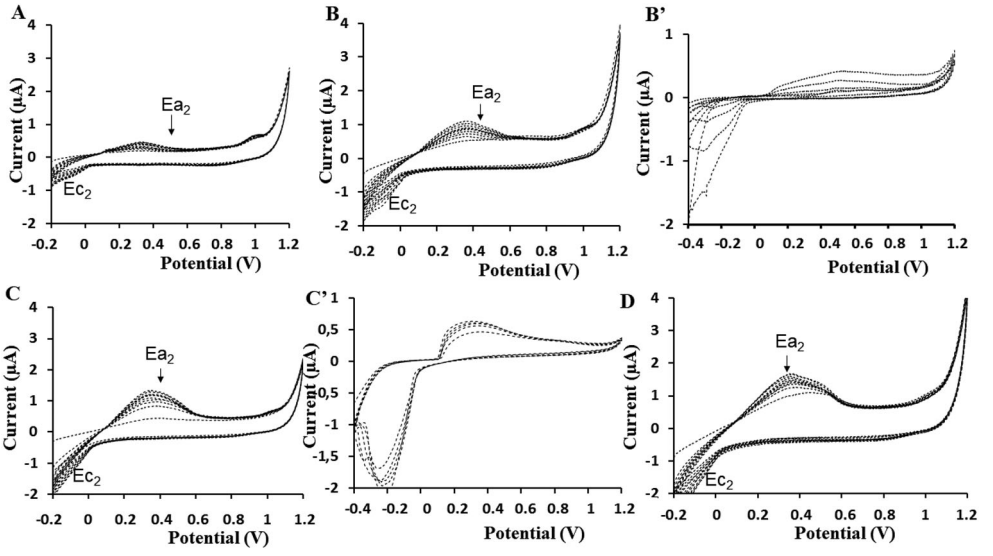

Figure 3. CV of HA6 (A), HA10 (B), HA12 (C) and HA17 (D); the HA solutions at 100 µM in KCl 1 M with 5% MeOH obtained at scan rate of 50 mV/s (10 cycles) from -0.2 to +1.2 V. Inserts (B′, C′): CV from -0.4 to +1.2 V of HA10 and HA12, respectively.

should be noted that the intensity of this redox couple (Ea_2/Ec_2) increased slightly with multiple scanning (Figure 3A–D).

A reversible redox process at the metal center was observed for Fe(II/III) and Cu(II) chlorides. However, Zn(II) and Ni(II) chlorides remained inert (Figure S5). For all Fe(II/III) complexes, a quasi-reversible peak within −0.2 V to +0.5 V was found. These processes

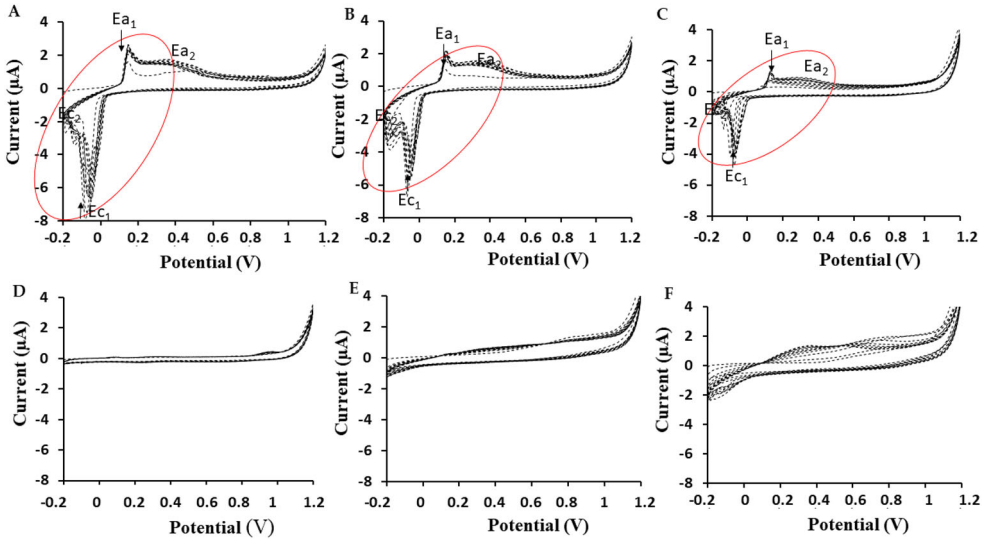

Figure 4. CV of HA17Fe2 (A), HA12FeCl (B), HA10Fe3 (C), HA17Cu2 (D), HA8Zn2 (E) and HA10Ni2 (F) at 100 µM in a 1 M KCl solution with 5% MeOH obtained at scan rate of 50 mV/s (10 cycles), potential ranges varied from -0.2 to +1.2 V.

Table 2. Crystallographic parameters and refinement data for HA8Fe3.

Crystallographic parameters		Crystallographic parameters	
Empirical formula	C_{24} H_{50} Fe N_3 O_7	Absorption coefficient (mm^{-1})	0.510
Formula weight	548.52	F(000)	1188
Temperature (K)	297(2)	Crystal size (mm^3)	0.30 × 0.17 × 0.03
Wavelength (Å)	0.71073	θ range for data collection	3.019 to 17.995°
Crystal system	Monoclinic	Reflections collected	7354
Space group	$P2_1/c$	Independent reflections	2187 [$R_{(int)}$ = 0.0913]
Unit cell dimensions (Å,°)	a = 17.575(2)	Completeness to θ = 17.995°	99.0 %
	b = 9.4793(5)	Max. and min. transmission	1.00000 and 0.95412
	c = 19.4493(14)	Data/restraints/parameters	2187/174/319
	β = 99.019(9)	Goodness-of-fit on F^2	1.073
Volume ($Å^3$)	3200.1(5)	Final R indices [I > 2sigma(I)]	R_1 = 0.0828, wR_2 = 0.1930
Z	4	R indices (all data)	R_1 = 0.1179, wR_2 = 0.2132
Density (calculated) (g/cm^3)	1.139	Dr $_{max/min}$ ($e^-.Å^{-3}$)	0.641 and −0.347

are identified by a red circle (Figure 4A–C). No redox peak at −0.2 V/+1.2 V was observed from the Cu(II) complexes (Figure 4D). While Zn(II) and Ni(II) complexes showed two broad redox peaks, *i.e.* a reduction starting at −0.2 V and an oxidation at +0.4 V, their intensities differed (Figure 4E,F).

3.2.6. Partition coefficients

The observed partition coefficients (Log P) were measured for all compounds and tend to increase with chain length (Figure S6).

3.2.7. X-ray diffraction

Attempts to obtain suitable crystals for X-ray diffraction analysis were unsuccessful for all complexes except for HA8Fe3, crystallographic parameters and refinement data are listed in Table 2. All heavy atoms were refined anisotropically and H-atoms were placed

in calculated positions with isotropic temperature factors fixed at 1.2 Ueq of the parent atoms (1.5 for methyl and O-H hydrogens). Although high resolution data were recorded, a resolution limit of 1.15 Å was imposed during refinement, beyond which poor data statistics were observed. The mobility of the alkyl chains is visible, showing an increase of the thermal ellipsoids moving along the alkyl chains towards the methyl ends. Rigid bond restraints on the thermal ellipsoids were applied on the last five atoms of all three alkyl chains. For every alkyl chain, the bond distances were restrained to be similar, no bond angle or torsion angles were restrained. One lattice water molecule is present (Figure 5) which corroborates the results obtained by KF analysis. Water stabilizes the molecular packing by hydrogen bonding between neighboring complexes (Figure S7.A). The hydrogen atoms of this water molecule were first located in the density maps, after which the water molecule was idealized and refined as a rigid group allowed to rotate around the oxygen atom. The conformation of each alkyl chain is different from the two others. A first one is fully elongated with all torsion angles eclipsed. A second chain starts with a gauche conformation, with the remaining torsion angles eclipsed. The third chain has three torsion angles in gauche conformation of which two are found consecutively. The hydrogen bonds propagate along the b and c axis forming a sheet-like structure, flanked by the apolar alkane chains (Figure S7.B).

A search in the CSD database reveals only one related structure (REFCODE SUXREI) [27]), equally a Fe complex with the shortest possible alkyl chain (methyl). The HA8Fe3 complex is arranged as a distorted octahedron (distortion parameter $\Sigma = 80.6°$) in the *mer* configuration, while in the crystal structure of SUXREI both the *fac* and *mer* configurations are present. The octahedral geometry of HA8Fe is comparable to the *mer* isomer of SUXREI ($\Sigma = 86.3°$, RMS deviation is 0.124Å^2 for the metal ion and the first coordination sphere, 0.217 Å^2 for all atoms in common (Figure S8).

Since crystals obtained for X-ray diffraction analysis exhibited no suitable diffraction patterns (except for HA8Fe3), DFT calculations were employed to uncover the local

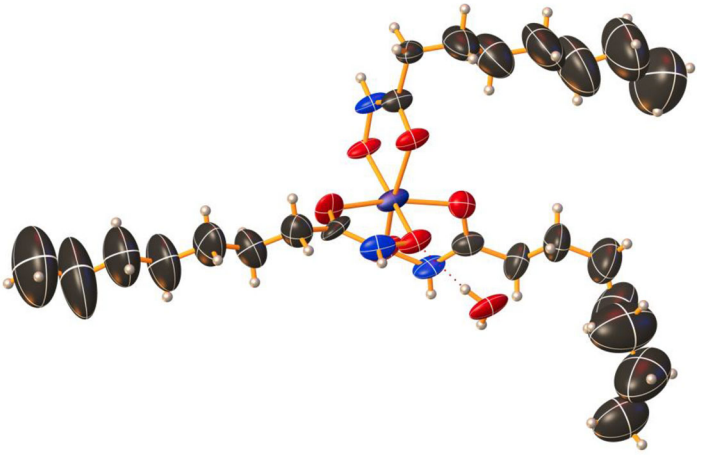

Figure 5. Thermal ellipsoid plots of complex HA8Fe3. All ellipsoids drawn at the 50% probability level. Colors are as follows: black, C; blue, N; red, O; grey, H; dark blue, Fe. CCDC 2079080 contains the supplementary crystallographic data for this paper. These data can be obtained free of charge from the Cambridge Crystallographic Data Centre via www.ccdc.cam.ac.uk/structures.

geometry around the metal centers. The DFT-optimized structures showed tetrahedral geometries for HA12Fe2, HA12Cu2 and HA12Zn2, and a square-planar geometry for HA12Ni2 (Figure S9).

CCDC 2079080 contains the supplementary crystallographic data for this paper. These data can be obtained free of charge from the Cambridge Crystallographic Data Centre via www.ccdc.cam.ac.uk/structures.

3.2.8. Stability

Stability analyses of HA by ^{1}H NMR showed no significant spectral modifications. Only NH and OH peaks disappeared for compounds HA2 and HA6 after 24 h (Figure S10). This should be due to proton exchanges of NH and OH with water in DMSO-d_6. Stability assays of complexes were monitored by UV-Vis spectroscopy. Compounds were dissolved in MeOH and water was added to reach the desired concentration for obtaining proper spectra. Significant changes with isosbestic points around 400 nm were observed after 10 minutes for HA2Fe3 (Figure S11.1A–D), HA2Ni2 (Figure S11.2A–E) and HA6Fe3 (Figure 6A–D). HA8Fe3 and HA12Fe3 showed neither significant absorption changes nor new absorption bands (Figures S11.1E–H and 6E–H). With other compounds, increased absorptions occurred during the test. This could be interpreted as the resolubilization of precipitated complex from the MeOH solution upon water addition rather than a degradation process. These results showed that the stability of compounds is influenced by the type of coordination metal and the length of the alkyl chain.

The change in absorbance over time at maximum wavelengths of HA6Fe3 showed hypsochromic and hyperchromic effects (λ at 350 and 380 nm). The appearance of isosbestic point after ten minutes could be due to an equilibrium between two species (Figure 7).

3.2.9. Magnetic susceptibility

Magnetic susceptibilities of the complexes were examined by measuring the magnetization of a dried sample at 300 K in a SQUID magnetometer (Table 3). All compounds

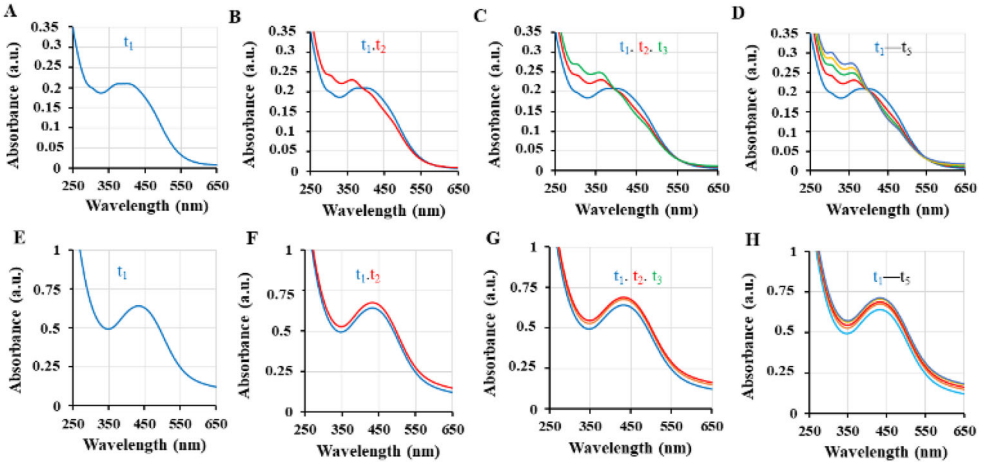

Figure 6. UV spectra of HA6Fe3 (A-D) and HA12Fe3 (E-H) aqueous solutions with 5% MeOH at 50 μM and at different times. t1 = 5 min, t2 = 10 min, t3 = 15 min, t4 = 20 min and t5 = 25 min.

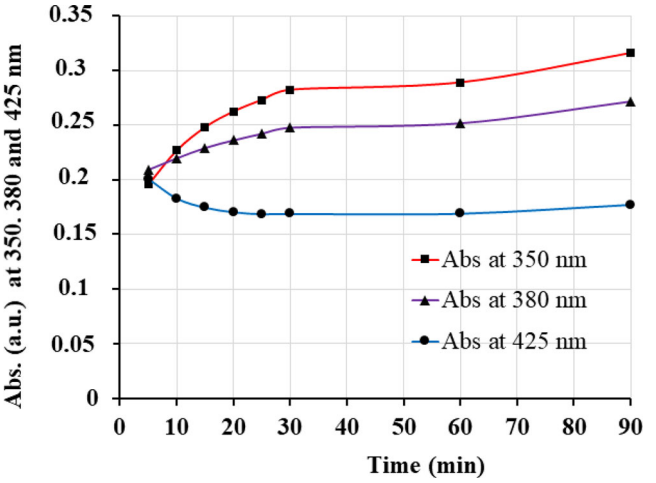

Figure 7. Changes in absorbance over time at 350, 380 and 425 nm of an aqueous 50 μM solution of HA6Fe3 with 5% MeOH during 90 minutes.

Table 3. Values of the mass susceptibility, molar mass, molar susceptibility and effective magnetic moment (μ_{eff}) of Fe(II/III), Ni(II), Cu(II) and Zn(II) complexes.

Complexes	Molar mass Kg mol^{-1}	Mass susceptibility $\times 10^{-8}$ m^3 Kg^{-1}	Mass susceptibility $\times 10^{-6}$ emu g^{-1} Oe^{-1}	Molar susceptibility $\times 10^{-8}$ m^3 mol^{-1}	Molar susceptibility $\times T \times 10^{-5}$ m^3 mol^{-1} °K	Effective magnetic moment μB
HA6Fe3	0.446	22.9	18.2	10.2	3.1	4.4
HA8Fe3	0.53	16.3	13.0	8.6	2.6	4.1
HA12Fe2	0.484	41.0	32.6	19.8	5.9	6.2
HA12FeCl	0.519	43.5	34.6	22.6	6.8	6.6
HA12Fe3	0.698	38.0	30.2	26.5	7.9	7.1
HA6Ni2	0.319	19.3	15.3	6.2	1.8	3.4
HA8Ni2	0.375	7.1	5.6	2.7	0.8	2.3
HA10Ni2	0.431	15.4	12.2	6.6	2.0	3.6
HA12Ni2	0.487	11.9	9.5	5.8	1.7	3.3
HA6Cu2	0.323	9.6	7.6	3.1	0.9	2.4
HA12Cu2	0.492	3.5	2.8	1.7	0.5	1.8
HA8Zn2	0.381	1.1	0.8	0.4	0.1	0.9
HA12Zn2	0.493	3.1	2.4	1.5	0.5	1.7

show paramagnetic behavior at room temperature, thereby variation in the mass susceptibility can be ascribed to the differences in the paramagnetic part in agreement with the nature of the compounds (Figure 8A–D).

3.2.10. Molar conductance

The measured molar conductance of HA, complexes and metal chlorides confirms their electrolytic character or not. HA and iron (II/III) complexes have quite low molar conductance values (0.63-5.63 $\Omega^{-1}cm^2mol^{-1}$) compared to $FeCl_2$ and $FeCl_3$ (around 90 $\Omega^{-1}cm^2mol^{-1}$). The molar conductance values of Ni(II) (28.17-37.11 $\Omega^{-1}cm^2mol^{-1}$), Cu(II) (21.79-24.32 $\Omega^{-1}cm^2mol^{-1}$) and Zn(II) (43.93-48.38 $\Omega^{-1}cm^2mol^{-1}$) complexes are relatively higher than Fe(II/III) complexes. However, they are weaker than the corresponding metal chlorides whose values are 82, 42 and 52 $\Omega^{-1}cm^2mol^{-1}$, respectively (Table 4).

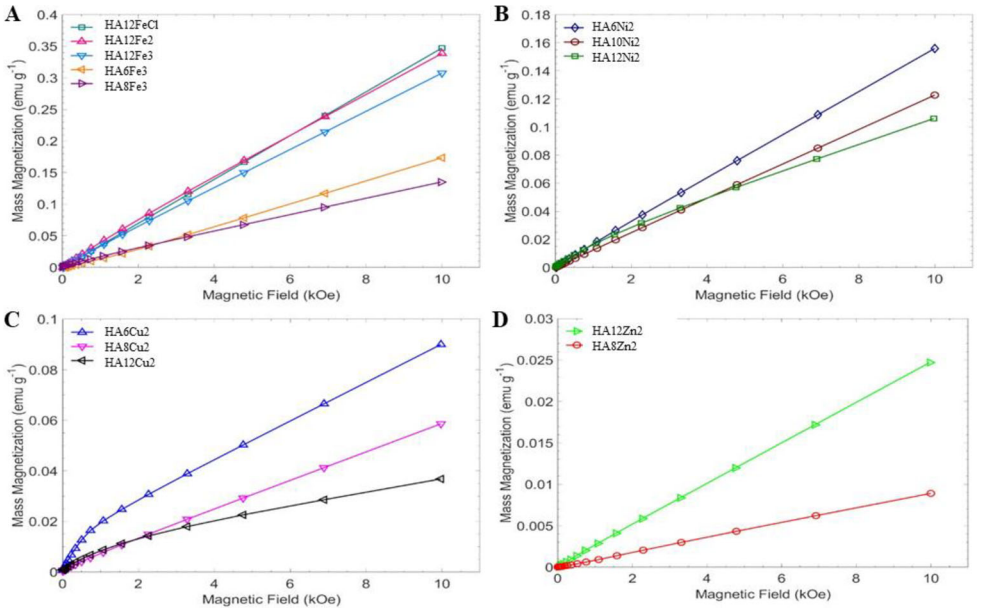

Figure 8. Room temperature hysteresis loops for (A-D) Fe(II/III), Ni(II), Cu(II) and Zn(II) based complexes, respectively. Iron complexes (A): HA6Fe3, HA8Fe3, HA12Fe2, HA12FeCl and HA12Fe3; nickel complexes (B): HA6Ni2, HA10Ni2 and HA12Ni2; copper complexes (C): HA6Cu2, HA8Cu2 and HA12Cu2; zinc complexes (D): HA8Zn2 and HA12Zn2.

Table 4. Values of electrical conductivity ($\Omega^{-1}cm^{-1}$) and molar conductance ($\Omega^{-1}cm^2mol^{-1}$) of HA, complexes and metal chloride.

	Concentration (mol/cm^3)		Conductivity in MeOH solution	
Compound	C_0	C_1	EC $\times 10^{-6}$ ($\Omega^{-1}cm^{-1}$)	MC ($\Omega^{-1}cm^2mol^{-1}$)
A2H	4.17×10^{-5}	2.09×10^{-6}	6	2.87
A6H	4.65×10^{-5}	2.33×10^{-6}	7	3
A8H	7.6×10^{-5}	3.8×10^{-6}	3	0.79
A12H	6.3×10^{-5}	3.16×10^{-6}	2	0.63
A6HFe3	1.07×10^{-5}	5.33×10^{-7}	3	5.63
A8HFe3	1.6×10^{-5}	8×10^{-7}	2	2.5
A12HFe2	1.06×10^{-5}	5.3×10^{-7}	2	3.77
A12HFe3	1.01×10^{-5}	5.05×10^{-7}	2	3.96
A10HNi2	5.68×10^{-6}	2.84×10^{-7}	8	28.17
A12HNi2	4.31×10^{-6}	2.16×10^{-7}	8	37.11
A8HCu2	6.58×10^{-6}	3.29×10^{-7}	8	24.32
A10HCu2	3.67×10^{-6}	1.84×10^{-7}	4	21.79
A12HCu2	5.99×10^{-6}	2.99×10^{-7}	7	23.36
A8HZn2	7.74×10^{-6}	3.87×10^{-7}	17	43.93
A10HZn2	7.44×10^{-6}	3.72×10^{-7}	18	48.39
A12HZn2	4.67×10^{-6}	2.34×10^{-7}	11	47.11
$FeCl_2$	8.07×10^{-5}	4.03×10^{-6}	365	90.57
$FeCl_3$	3.53×10^{-5}	1.77×10^{-6}	160	90.39
$NiCl_2{\cdot}6H_2O$	2.09×10^{-4}	1.05×10^{-5}	860	81.9
$CuCl_2{\cdot}2H_2O$	2.7×10^{-4}	1.35×10^{-5}	563	41.7
$ZnCl_2$	6.8×10^{-5}	3.41×10^{-6}	177	51.91
MeOH	–	–	1	–

C_0: initial concentration, C_1: final concentration studied (C_0 diluted 20 times), EC: electric conductivity (measurement using a conduct), MC: molar conductance (calculated by the EC/MC ratio)). MeOH: blank.

3.3. Biological activity

3.3.1. Antimicrobial effect

The MIC and the MBC/MFC were determined using Gram positive bacteria (methicillin-sensitive/resistant *S. aureus*, *C. glutamicum*, *B. subtilis*), Gram negative bacteria (*E. coli*, *P. aeruginosa*, *K. pneumoniae*), mycobacteria (*M. smegmatis*) and fungi (*C. albicans*). The concentration ranges of tested samples were between 16 μM − 3 mM. The antibacterial activity has been defined as significant when the MIC is below 20 μM (between 2-20 μg/mL depending on the compound), moderate when $20 < \text{MIC} < 200\,\mu M$, low when $200 \leq \text{MIC} < 500\,\mu M$ and insignificant when MIC $> 500\,\mu M$, range in μg/mL depending on the chemical compound [49] (Table S3).

Most of the compounds, such as HA2, HA6, HA8 and HA17, did not show any effect on the tested microbial strains (Table S3). HA10 showed moderate activity towards *C. albicans* (MIC = 31 μM) while HA12 showed stronger activity against *C. albicans* (MIC = 16 μM) and moderate activity against *S. aureus* MSSA/MRSA, *C. glutamicum*, *B. subtilis*, *E. coli* and *M. smegmatis* (MIC between 63-125 μM). However, it was inactive against *P. aeruginosa* and *K. pneumoniae* (Table S3). Moderate antimicrobial effects were also observed with Fe(II/III) and Zn(II) complexes such as those derived from HA6 (HA6FeCl, HA6Fe3, HA6Zn2), from HA8 (HA8Zn2), from HA10 (HA10Fe2, HA10FeCl, HA10Fe3, HA10Zn2) and from HA12 (HA12Fe2, HA12FeCl, HA12Fe3, HA12Zn2), against *S. aureus* MSSA, *E. coli* and *C. glutamicum* (Table 5 and Figure S16). However, the antibacterial activity of $ZnCl_2$ against *E. coli* (MIC < 78 μM) was better than HAnZn2 and the HA12 was always more active than HAnFe2, HAnFeCl, HAnFe3 and HAnZn2. HAnNi2 and HAnCu2 were generally inactive except for HA12Cu2 and HA12Ni2 that inhibited *C. albicans* growth, having similar or even slightly increased MIC (16 and 31 μM, respectively) compared to HA12 (MIC = 16 μM). *C. albicans* was also similarly susceptible to HA12Zn2 (MIC = 16 μM). HA12 derived complexes HA12Fe2, HA12FeCl, and HA12Fe3 were moderately active against *M. smegmatis*, with HA12Fe3 being more active (31 μM) than HA12 (MIC = 63 μM).

Selected compounds were further evaluated for bactericidal/fungicidal activities (Table S4 and Figure S17). Their MFC or MBC were generally obtained at concentrations reaching two-three times the MIC. The fungicidal activity (MFC of 31 μM) of HA12 and HA12Zn2 on *C. albicans* was particularly relevant.

The most active compounds HA12, HA12Fe2, HA12FeCl, HA12Fe3, HA12Cu2, HA12Zn2 and HA12Ni2 were further purified and re-tested (see Appendix A). Results of biological re-evaluations were similar to those obtained during the initial screening.

3.3.2. Cell viability effect on SiHa cells

Cytotoxicities of HA6Fe3, HA8FeCl, HA8Fe3, HA10FeCl, HA10Fe3, HA12, HA12Fe2, HA12FeCl, HA12Fe3, HA12Cu2, HA12Zn2 and HA12Ni2 were determined on SiHa cells (human cervical cancer cell line) and reported in Figure S18. The IC_{50} values of these twelve compounds were reported (Table 6). Those obtained with HA12Fe2, HA12FeCl and HA12Fe3 were approximately the same (Table 6).

The SI of the antimicrobial activities of these compounds with regards to their human cell line cytotoxicity were determined by calculating their IC_{50}/MIC ratio. Compounds having a high IC_{50} and a low MIC were considered the most interesting ones, as they

Table 5. Most significant MIC values (in μM and/or μg/mL) of selective antimicrobial HA and their complexes against bacteria, mycobacteria and yeast.

	Gram- positive bacteria								Gram- negative bacteria						Mycobacteria		Yeast	
	MSSA		MRSA		*Cg*		*Bs*		*Ec*		*Pa*		*Kp*		*Ms*		*Ca*	
Code	μM	μg/mL	μM	μg/mL	μM	μg/mL	μM	μg/mL	μM	μg/mL	μM	μg/mL	μM	μg/mL	μM	μg/mL	μM	μg/mL
HA10	313*	58	>500**	>934	500**	>94	>500*	>94	313*	58	>500**	>94	>500**	>94	>500**	>94	**31#**	**6**
HA10Fe2	**125***	**56**	>500**	>223	**125****	**56**	>500**	>223	>500**	>223	>500**	>223	>500**	>223	>500**	>223	>500**	>223
HA10FeCl	**78***	**38**	>500**	>2401	250**	120	>500**	>241	313**	151	>500**	>240.8	>500**	>241	>500**	>241	>500**	>241
HA10Fe3	**78***	**49**	>500**	>316	**125****	**79**	>500**	>316	**<78****	**<49**	>500**	>316	>500**	>316	>500**	>316	>500**	>316
HA12	**63***	**13**	**125#**	**27**	**63***	**13**	**62.5***	**13**	**63***	**13**	>500**	>108	>500**	>108	**63***	**13.44**	**16#**	**3**
HA12Fe2	>500**	>251	>500**	>251	>500*	>251	**125****	**63**	>500**	>251	>500**	>251	>500**	>251	**125****	**63**	>500**	>251
HA12FeCl	>500**	>269	>500**	>269	>500*	>269	250**	135	>500**	>269	>500**	>269	>500**	>269	**125****	**67**	>500**	>269
HA12Fe3	>500**	>358	>500**	>358	>500*	>358	**125***	**90**	**156***	**112**	>500**	>358	>500**	>358	**31***	**22**	>500**	>358
HA12Cu2	>500**	>246	>500**	>246	>500*	>246	>500*	>246	>500	>246	>500**	>246	>500**	>246	>500**	>246	**16****	**8**
HA12Zn2	>500**	>247	>500**	>247	>500**	>246	>500**	>247	**156****	77	>500**	>247	>500**	>247	>500**	>247	**16****	**8**
HA12Ni2	>500**	>244	>500**	>244	>500**	>243	>500**	>244	>500**	>244	>500**	>244	>500**	>244	>500**	>244	**31****	**15**

MIC values of the most active compounds are in bold; vancomycin (vanc), cetrimide (cetr) and rifampicin (rifa) were used as positive controls. MSSA/MRSA = methicillin-sensitive/resistant S. aureus, Cg = C. glutamicum, Bs = B. subtilis, Ec = E. coli, Ms = M. smegmatis, Ca = C. albicans. Control with 5% of both DMSO and MeOH in water have been done and microbial growth was observed in these solvents. * $p \leq 0.05$; ** $p \ll 0.05$ and # $p > 0.05$ (in the μM column) obtained by t-test (see SI, Table S3.3–table S3.5).

Table 6. MIC, IC_{50} (μM) and the SI of Compounds with significant inhibitory effects. SiHa: human cervical cancer cell line.

	Bacteria										Mycobacteria		Yeast		Cancer cells
	MSSA		MRSA		Cg		Bs		Ec		Ms		Ca		SiHa
Code	MIC	SI	MIC	SI	MIC	SI	MIC	SI	MIC	SI	MIC	SI	MIC	SI	IC_{50}
HA6Fe3	78	0.04	–	–	–		–	–	–	–	–	–	–	–	3
HA8FeCl	78	0.76	–	–	–		–	–	156	0.38	–	–	–	–	59
HA8Fe3	78	0.10	–	–	–		–	–	156	0.38	–	–	–	–	8
HA10FeCl	78	0.39	–	–	–		–	–	–	–	–	–	–	–	30
HA10Fe3	78	0.40	–	–	–		–	–	78	0.40	–	–	–	–	31
HA12	63	0.26	125	0.13	63	0.26	63	0.26	63	0.26	63	0.26	16	1.02	16
HA12Fe2	–	–	–		–		125	0.40	–	–	125	0.40	–	–	50
HA12FeCl	–	–	–		–		–	–	–	–	125	0.38	–	–	48
HA12Fe3	–	–	–		–		125	0.39	156	0.31	31	1.56	–	–	49
HA12Cu2	–	–	–		–		–	–	–	–	–	–	16	5.11	80
HA12Zn2	–	–	–		–		–	–	156	0.37	–	–	16	3.74	58
HA12Ni2	–	–	–		–		–	–	–	–	–	–	31	1.60	50

show together low cytoxicity and high antimicrobial activity. The ratios were rather similar when considering the antimicrobial activities against *S. aureus* MSSA, *C. glutamicum*, *B. subtilis*, *E. coli* and *M. smegmatis* strains (0.26) (Table 6). The best antimicrobial selectivities were observed for HA12Cu2 (SI = 5.11), HA12Zn2 (SI = 3.74) and HA12Ni2 (SI = 1.60) on *C. albicans* (Table 6), having higher IC_{50} compared to their MIC.

4. Discussion

4.1. IR spectroscopy

Spectral analyses confirmed the identity of the HA and their complexes. IR spectra revealed the presence of HA in their deprotonated form in the complexes. Water molecules within the coordination sphere of Fe(II/III) complexes was identified by broad bands in the region 3450-3250 cm^{-1} due to O-H stretch [9]. With Zn(II) and Ni(II) complexes, the bands observed in the same region are very weak and even absent for Cu(II) complexes, which corroborate the results of the water determination by the KF titration. A sharp band at 1619-1662 cm^{-1} with HA, in the region 1520-1595 cm^{-1} for the Fe(II/III) complexes, and at 1539-1599 cm^{-1} for those of Cu(II), Zn(II), Ni(II) is attributed to the shifted vibration frequency of C = O upon complexation. This band undergoes a shift to lower wavenumber as described elsewhere [31, 48], which is consistent with the chelation by the carbonyl oxygen atom. The C-N bands are found at 1459-1499 cm^{-1} upon complexation. Regarding the M-O stretching vibrations we observed several bands between 400 and 600 cm^{-1}, depending on the metal, that confirmed the chelated structure [31, 48, 50–52].

4.2. UV spectroscopy

In the UV spectra (Figure 1), a slight bathochromic and medium hyperchromic displacement characteristic of the tri-coordinated Fe(III) complex (HA10Fe3) appears compared to the di-coordinated Fe(II) complex (HA10Fe2, $\Delta\mathcal{E} = 750\ M^{-1}cm^{-1}$). Between the complexes of HA10FeCl and HA10Fe3, a large hyperchromic displacement of

1670 $M^{-1}cm^{-1}$ is observed. This variation of $\mathcal{E}$ is influenced by the nature of the coordinating metal. Moreover, the variation of absorbance is an important factor in determining the stoichiometry of the complexes. The wavelength corresponding to the maximum absorption depends on the mode of coordination of the metal ion and stoichiometry (1 metal for 2 HA or 1 metal for 3 HA) and is independent of the nature of the HA [53].

The electronic transitions $n \rightarrow \pi^*$ (C = O) observed show a bathochromic shift towards a higher wavelength. This indicates that complexation has occurred between HA and the corresponding metal chloride [54]. The absorption maximum at 425 nm characterizes the ligand-metal charge transfer bands of complexes HAnFe2, HAnFeCl and HAnFe3 [55], those of HAnNi2 and HAnCu2 at $\lambda_{max} = 250$ nm (Figures 1 and S4).

4.3. Cyclic voltammetry

Additional characterization by CV allowed us to obtain the electrochemical features of our synthesized molecules. CV of HA showed a first irreversible anodic peak (Ea_1), assigned to a one-electron oxidation of the hydroxamato group leading to formation of a transient nitroxide radical. It can be seen that the longer the alkyl chain, the lower this oxidation potential Ea_1. This could be due to the donor effect of the alkyl chain, although this effect can be considered as weak when the chain is longer than five methylene groups. Then, different oxidation pathways have been suggested with either the formation of an acyl radical intermediate with the loss of one electron or the formation of an acyl nitroso, both hydrolyzing into their respective carboxylic acids with the release of a molecule of NHO (Scheme 3A) [56, 57]. This latter is unstable and dimerizes leading to formation of N_2O and H_2O (Scheme 3B) [56–58]. According to previous publications [58–60], this oxidation pathway is even more complex and can lead to formation of the respective *N,O*-diacylhydroxylamine by recombination of either the acyl radical with the nitroxide radical or by reaction between the acyl nitroso with the deprotonated form of HA (Scheme 3C).

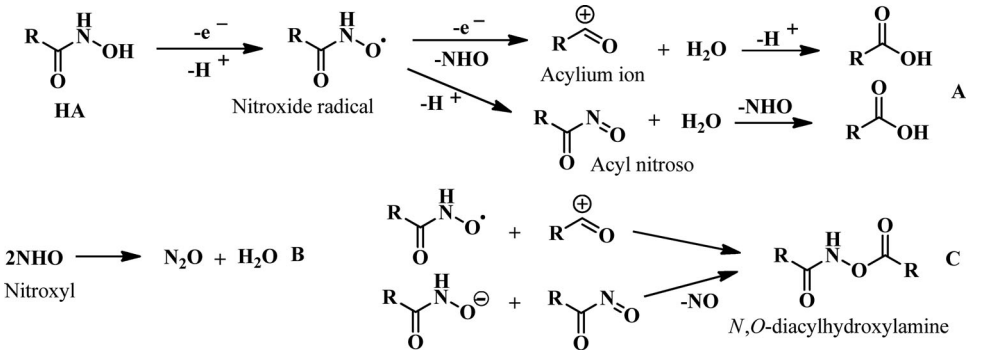

Scheme 3. Proposed electrochemical mechanism of HA onto carbon screen-printed electrode (cSPE). A. Decomposition of HA into nitroxide radical derived from one electron oxidation to give acylium ion or acyl nitroso which hydrolyzes in RCOOH. B. Unstable NHO dimerizes into N_2O and H_2O. C. Possible oxidation pathway by recombination of acyl radical with the nitroxide radical or acyl nitroso with deprotonated HA to give *N,O*-diacylhydroxylamine.

The hydroxamate group may also be reduced, although this reduction is hardly described in the literature. According to the CV of aliphatic HA and by comparing them with data published on aromatic HA, it could be postulated that the mechanism is closer to the reduction of *N*-hydroxy-2-oxo-2-phenylacetamide (PhCOCONHOH) into 2-hydroxy-2-phenylacetamide ($PhCHOHCONH_2$) and 2,3-dihydroxy-2,3-diphenylsuccinamide ($[PhC(OH)CONH_2]_2$) [61], and that may explain the appearance of the reversible redox couple (Ea_2/Ec_2) observed at −0.2 V and +0.4 V with HA.

Regarding the Cu(II) complexes, the absence of electrochemical processes could be explained by their greater electrochemical stability in KCl aqueous solution (1 M) in 5% MeOH on the carbon screen-printed electrode (cSPE) surface than the other studied complexes (Figures 4 and S11). For the Zn(II) and Ni(II) complexes, the redox process can be assigned to the electrochemical phenomenon on the HA itself meaning that those complexes are more unstable in those conditions. The CV of Fe(II/III) complexes reveal a quasi-reversible redox process with absorption phenomenon involving likely the HA itself and the central metallic atom. The well-defined reversible peaks at Ea_1 (+0.1 V) and Ec_1 (-0.1 V) are due to the redox process of the Fe center [62]. Compared to the reversible redox peak at +0.9 V for iron chloride (Figure S5), those peaks are shifted to a lower value of potential, indicating a facilitated electron transfer in those complexes. Finally, the broad anodic peak at +0.3 V and the broad cathodic peak at −0.2 V are linked to the electrochemical reaction of the HA.

4.4. Stability of compounds

Concerning the stability of HA in water, hydrolysis into carboxylic acid and hydroxylamine is the main degradation pathway described in the literature. This hydrolysis is very slow in a neutral aqueous solution compared to an acidic medium, by several orders of magnitude [63, 64]. The non-catalyzed hydrolysis of HA in water is extremely slow and insignificant [64], hence HA are expected to be stable. Ligand-water molecule exchange is the expected reaction that could occur with complexes. The stability study of our complexes using UV-visible spectrophotometry revealed that only HA2Fe3 and HA6Fe3 are clearly unstable in water. After about 20 minutes, strong changes appeared in the UV-visible spectra. According to previously published work, the degradation products could be carboxylic acid and NH_2OH through hydrolysis, and Fe^{3+} by decomplexation. The hydrolysis rate of Fe(III) complexes is greater than that of their corresponding HA [63, 64]. Data found in the literature highlighted two structural elements related to the stability of the HA complexes: (i) the type of coordination metal and (ii) the length of the alkyl chain [65, 66]. Regarding the metal, the size of the cation influences the stability: the smaller the cation, the higher stability (following the Irvings-Williams order of stability: $Fe^{2+} < Ni^{2+} < Cu^{2+} < Zn^{2+}$). The chain length is cited as a factor influencing the stability but with no explanation.

4.5. Magnetic susceptibilities and electrolytic characteristics of complexes

The susceptibility of the different complexes at room temperature (Figure 8A–D) show paramagnetic behavior. Although a diamagnetic component in the susceptibility does

not change much, it could also be present in the compounds. As seen from Table 3, Cu(II) and Zn(II) complexes show lower susceptibility values compared to Fe(II/III) and Ni(II) complexes, from which HA12FeCl complex demonstrates the largest value of mass susceptibility (34.64×10^6 emu g^{-1}) in agreement with the previous report on ferric compounds [67]. The ratios between mass susceptibilities for Fe(II/III), Ni(II), Cu(II) and Zn(II) complexes are comparable with those between molar susceptibilities for related inorganic compounds, *i.e.* $\chi_m = +13450, +6145, +1080, -55 \times 10^{-6}$ cm^3 mol^{-1} for $FeCl_3$, $NiCl_2$, $CuCl_2$, $ZnCl_2$, respectively [35]. It can be seen in Figure 8B,C that a dominant ferromagnetic/superparamagnetic-like contribution is observed for some Cu(II) complexes as well as HA12HNi2 complex at room temperature. Hence a small room temperature coercive field ($H_c = 63$ Oe) and remanence ($M_r = 8 \times 10^{-4}$ emu g^{-1}) for the HA12Cu2 complex (Figure S19) are observed, probably an effect of magnetic contamination. Interestingly, a paramagnetic dependence is observed for Zn(II) complexes (Figure 8D) for one would expect prevailing diamagnetism featured in Zn inorganic compounds.

The highest magnetic moment (μ_{eff}) values were obtained with the Fe(II/III) complexes which are between 4.41-7.12 BM (Table 3). The Ni(II) complexes show μ_{eff} values between 2.25-3.55 BM corresponding to two unpaired electrons (d^8). Those of Cu(II) ($\mu_{eff} = 1.82$-2.43 BM) are in agreement with a structure bearing one unpaired electron (d^9) [68, 69]. As for the Zn(II) complexes, the values were between 0.89-1.69 BM. This is in accord with data published, for instance with the triazole complexes of Fe ($\mu_{eff} = 5.06$ BM), Ni ($\mu_{eff} = 2.97$ BM) and Cu ($\mu_{eff} = 1.79$-1.81 BM) [5]. These values indicate that these complexes are paramagnetic. The values of μ_{eff} for triazole Zn(II) complexes is close to 0 BM, corresponding to diamagnetic complexes [5, 70]. These data allow correlating the magnetic properties of the complexes with the configuration of the d^6, d^8, d^9 (paramagnetic: Fe(II/III), Ni(II), Cu(II), respectively) and d^{10} orbitals (diamagnetic: Zn(II)). Overall, the magnetic properties of the investigated complexes correlate well with the values of molar magnetic susceptibilities of their inorganic counterparts and effective magnetic moments of similar complexes.

In the literature, molar conductance values between 11-19 $\Omega^{-1}cm^2mol^{-1}$ indicate an absence of ionic form of the complexes in solution. For instance, a conductivity value of 98 $\Omega^{-1}cm^2mol^{-1}$ obtained with a chromium(II) complex with a triazole ligand was considered to be a confirmation of its ionic character (electrolyte) [70]. Results obtained with our Fe(II/III), Ni(II) and Cu(II) complexes versus $FeCl_2$, $FeCl_3$, $NiCl_2$ and $CuCl_2$ thus corroborate their non-ionic nature. As for the Zn(II) complexes, the value of their molar conductance is close to that of $ZnCl_2$, suggesting an ionic character (Table 4). In another published work, complexes of Ni(II), Cu(II) and Zn(II) with Schiff bases (sulfanilamides) have shown molar conductance values in dimethylformamide (DMF) between 135-142 $\Omega^{-1}cm^2mol^{-1}$, indicating the electrolytic nature of these complexes [71].

4.6. Antimicrobial effect and cytotoxicity

Vancomycin, rifampicin and cetrimide (reference antibiotics and antiseptic) showed a greater inhibitory effect than HA and Fe(II/III), Ni(II), Cu(II) and Zn(II) complexes.

Although the antimicrobial effects observed are weaker than those of standard antibiotics, a higher inhibition than other compounds described in the literature is observed. The antimicrobial results obtained with compound HA12 (13.44 μg/mL) are more significant than those obtained with *N*-(2-hydroxyethyl)-5-nitrosalicylaldimine (MIC = 250 μg/mL) on the same strains (SASM and *E. coli*). Although the HA and complexes of the present work were inactive against *K. pneumoniae* and *P. aeruginosa* (MIC > 0.5 mM), previously described Cu(II) complexes with Schiff base ligands showed an inhibitory effect against these two bacterial strains (MIC = 2.4-5.8 mM) [72]. The HA12Ni2 (MIC = 15 μg/mL), HA12Cu2 and HA12Zn2 (8 μg/mL) complexes which were the subject of our study have a more significant antifungal effect than the Fe(II) and Ni(II) complexes of *N*-(2-hydroxyethyl)-5-nitrosalicylaldimine (MIC = 250 μg/mL) against *C. albicans* [73].

Other examples confirm our results on the antifungal activity observed. This is the case for Cu(II) complexes of 1,10-phenanthroline and 2,2′-bipyridine (MIC = 1000 μg/mL) against *C. albicans* [74]. In addition, the HAnZn2 complexes (n = 6, 8, 10 and 12) active against *E. coli* have lower MIC than Zn(II) complexes of mono and dinitrobenzohydroxamate (MIC = 100 μg/mL and > 200 μg/mL, respectively) on the same strain [7]. The HA12Fe3 complex is more active (MIC = 22.38 μg/mL, *M. smegmatis*) than the Co(II) and Cu(II) complexes of benzohydroxamate against *M. tuberculosis* (MIC = 50 and 100 μg/mL, respectively) [14].

Although HA displayed antimicrobial activities [4, 75, 76], the effect of the length of the alkyl chain has not been studied in the literature [77]. In our study, compounds which have a significant antimicrobial effect on the microorganisms tested are those having a logP ≥ 3 (HA12 and corresponding complexes) (Figure S6). This points out the hydrophobic character as an important factor for antimicrobial activity thanks to a better diffusion through the cell membrane [78, 79]. A correlation between the alkyl chain length and the antibacterial or antifungal effect of the hydrophobic compounds HA10 and HA12 has been observed (Table S3) with a two-fold lower MIC for HA12 on *C. albicans* compared to HA10. However, HA12 is moderately active on *E. coli* with MIC at 63 μM (13 μg/mL) and HA17 is inactive against the same strain, highlighting that water solubility is also a significant parameter. Consequently, there is a need for a good balance between these two properties. For instance, it was reported that the *N*-acetoxy palmitoylhydroxamic acid has no significant effect on *E. coli* [80], probably due to low water solubility.

Compared with HA6 and HA8, their derived complexes with Fe(II/III) or Zn(II) (HAnFe2, HAnFeCl, HAnFe3, HAnZn2) displayed stronger inhibition against *S. aureus* and *E. coli*, in agreement with the report that the antimicrobial activity of HA complexes was higher than the corresponding free HA [8]. Cell wall penetration in Gram negative bacteria is lower than in Gram positive bacteria, due to the fact that the outer membrane of the Gram negative bacteria limits the diffusion of compounds inside the cytoplasm [78, 79]. Lipophilic ligands could facilitate the penetration of the metals through the hydrophobic lipid layer, explaining thus the increase in antimicrobial activities for most lipophilic molecules [81]. The increased activity of the complexes compared to their respective HA is often explained by Overton's concept and Tweedy's chelation theory [72]. According to the Overton's concept of cell

permeability, the lipid membrane surrounding the cell favors the passage of only fat-soluble materials. During chelation, the polarity of the metal ion is reduced due to the neutralization of the positive charge with the negatively charged donor groups of the ligands. This improves the lipophilic character of the metal atom in the complex compared to the metal alone. Penetration through the lipid layers of the cell membrane is facilitated by this lipophilicity [82].

Compounds HA10 and HA12 displayed antimicrobial effect on *C. albicans*, showing a fungistatic activity for HA10 and fungicidal activity for HA12. HA12, HA6FeCl, HA6Fe3, HA8FeCl, HA8Fe3, HA10Fe2, HA10FeCl and HA10Fe3, HA6Zn2, HA8Zn2, HA10Zn2, HA12Zn2 and zinc chloride also demonstrated bactericidal activity against *S. aureus* MSSA, *C. glutamicum* and *E. coli*. HA12 had a broad spectrum of antimicrobial activities, being active not only against fungi, Gram positive and negative bacteria but also against drug resistant MRSA and *M. smegmatis*. On the opposite, its derived complexes, HA12Cu2, HA12Zn2 and HA12Ni2, were mainly active against *C. albicans*. As previously published, Fe(II/III), Ni(II), Cu(II) and Zn(II) complexes of HA displayed various antibacterial and antifungal activities [8–11]. For the moment, the mechanisms of action of these compounds are not known but some hypotheses could be proposed, based on the chemical properties of HA and the metals used in this study.

Compounds such as HA could inhibit microorganisms through metal chelation involved in enzymatic reactions but also through their ability to release HNO and NO, as shown in CV analysis [83]. Fosmidomycin, an antibiotic from *Streptomyces*, derived of *N*-hydroxyhexanamide, is a good example of a natural HA targeting a metal containing enzyme in bacteria. Indeed, it is able to inhibit DXP reductoisomerase whose activity depends on Mn^{2+}, Co^{2+} or Mg^{2+} ions [84]. In the case of metal complexes, either small amount of metal arising from complex dissociation or the metal complexes themselves could produce deleterious biochemical effects on microorganisms. It remains difficult to determine precisely the mechanism of action of such species in complex biological systems, but it is logical to consider that metal ions could combine with the chemical groups present in proteins, mainly SH, COO^- and imidazoles, such as those present in ribosomes [84]. Other hypotheses on the mode of action include inhibition of DNA synthesis, cell wall or membrane disruption or inhibition of RNA synthesis based on a disturbance in the energy metabolism of the cell. Finally, disruption of the membrane could affect the electron transport chain and the oxygen consumption of microorganisms. However, some compounds could also act outside the cytoplasm. Pathogens secrete various molecules (small ones or proteins) to achieve some metabolic pathways at the membrane periphery, as exemplified by bacterial transpeptidases that are inhibited by beta-lactam antibiotics.

Some compounds were mostly inactive on a drug resistant *S. aureus* strain. This could be due to the higher cell wall hydrophobicity of this strain [85]. The broad antimicrobial spectrum activity of HA12 could be due to the fact that this compound could chelate different metals in the various tested microorganisms [77]. The increased antifungal activity of HA12 derived complexes could be due to their ability to trigger cell death when they get attached to the negatively charged microbial cells and can cause irreversible cell membrane damage [86].

HAnZn2 and $ZnCl_2$ have stronger inhibitory effects than other complexes (HAnFe2, HAnFeCl, HAnFe3, HAnCu2 and HAnNi2) on *E. coli*. HAnZn2 displayed growth inhibition with a MIC of 78 μM, higher than the MIC of $ZnCl_2$ (< 78 μM) on *E. coli* (Table S3), indicating that complexation is not always necessary for the metal to exert its biological activity. A good example is ZnO nanoparticles that can cause membrane disorganization and, subsequently, destruction of intracellular components of *E. coli* [87]. The HA12 complexes showed a particular antifungal activity on *C. albicans*, with stronger activity for HA12Cu2 and HA12Zn2 than HA12Ni2, probably due to the difference in standard reduction potentials. Indeed, the CV assay values and UV stability studies indicated that HAnCu2 are more stable than those of HAnZn2 or HAnNi2 (Figures 4 and S11). Our hypothesis is that Zn(II) or Ni(II) could be reduced in fungi's cytoplasm and lose more easily their ability to bind the targets. In other words, reactivity of the complexes could improve their antifungal activity [12]. The lipid, carbohydrate or protein contents in microorganism membranes, and consequently, their physicochemical properties, could explain the specificity of the HA derived complexes on the different microorganisms. The hydrophobicity of the compounds, along with the nature of the metal in the complexes, is thus only one of the factors that could explain specific antimicrobial properties [77, 88].

Selectivity towards human cells was a major concern for a potential use of the complexes in medicine. In this view, SI were determined. Antifungal compounds HA12Cu2, HA12Zn2 and HA12Ni2 showed better selectivities compared to HA12 (Table 6). The broad activity spectrum of HA12 could be due to its pleiotropic action on microorganism and human cells based on metal complexation. However, Fe(II/III) complexes with a shorter alkyl chain (hydrophilic) were more cytotoxic on SiHa cells than their higher lipophilic homologues. The complexes HA6Fe3 and HA8Fe3 showed the highest cytotoxicities with SI of 0.04 and 0.10, respectively. These hydrophilic complexes could be more easily localized in the cell nucleus or in the mitochondria and therefore induce cell cycle arrest by triggering DNA damage. Previous work on HA reported that their toxicity could result from iron ion withdrawal by chelating, which could greatly reduce DNA synthesis and cell growth [89]. They could also be competitive inhibitors of transferrin [90].

The results on the antimicrobial effect of some compounds provide interesting data, especially the HA12, HA12Ni2, HA12Cu2 and HA12Zn2 showing significant fungicidal activity against *C. albicans*. Further studies must be undertaken to assess their potential medical interest (as disinfectant for instance) and to determine their mechanism of action.

5. Conclusion

HA and their Fe(II/III), Ni(II), Cu(II) and Zn(II) complexes were synthesized, characterized and evaluated for their antimicrobial properties against various microorganisms. As expected, a correlation was found between the lipophilicity of the HA and derived complexes (HAnFe2, HAnFeCl, HAnFe3, HAnNi2, HAnCu2 and HAnZn2) (expressed as their logP) and their antimicrobial effects and cytotoxicities [81, 91]. A similar correlation was found between their molecular weights and antimicrobial activities. The

lipophilic complexes HA12Cu2, HA12Zn2 and HA12Ni2 have interesting antifungal activity, considering their selectivity index. On the opposite, HA12 has a broad spectrum of antimicrobial activities but is also equally toxic on human cell lines. Altogether, our results suggest that HA and in particular, their complexes, could be used for the development of novel antimicrobial and particularly antifungal compounds, as surface coating agents or as disinfectants.

Acknowledgements

We are grateful to Corenthin Mees, François Xavier Nshimiyimana and Prof. Jean-Michel Kauffmann for their help in achieving experimental procedures described in the paper. We thank Sofia Oliveira for providing some bacteria strains; the analytical platform of the Faculty of Pharmacy (ULB) for MS analyses and fruitful discussions (P. Van Antwerpen, F. Reyé and C. Delporte); the Centre d'Instrumentation en Resonance Magnétique (CIREM) and High-Resolution NMR laboratory (ULB) for the NMR and EPR experiments (M. Luhmer and G. De Leener); the "service de traitement des eaux et pollution de l'école polytechnique de Bruxelles" (M. Verbanck and J. Schneider) for electrical conductivity measurements; the PC2 platform for elemental analyses (UNamur) and J.-F. Statsyns (UCLouvain) for the Raman spectra. I.-S. Sow thanks Abdoulaye Yéro Baldé, the former minister of higher education and scientific research of Guinea for his financial support. We thank L. M. C. Pereira for help in analyzing the magnetic measurements.

Disclosure statement

No potential conflict of interest was reported by the authors.

Funding

The magnetic analyses were supported by the Research Foundation – Flanders (FWO) and by the KU Leuven C1 program (Grant No. C14/18/074).

Author contributions

Conceptualization, methodology, investigation, writing—original draft preparation, data curation, and all chemical analysis—biological assay, I.S.S.; CV and KF analysis, M.V.; review and supervision, F.M.; crystallization assay and DFT calculations, M.M.; DFT calculations and review, G.B; crystal assay, K.R.; Raman analysis and review, S.H.; data curation and review, D.Y.; magnetic analysis, S.B., M.J.V.B; visualization, supervision, review, validation chemical analysis—biological assay, M.G., V.F. and F.D. All authors have read and agreed to the published version of the manuscript.

ORCID

Sophie Hermans http://orcid.org/0000-0003-4715-7964

References

[1] M.A. Agrawal, J. Harjit, R. Pande. *J. Phys. Org. Chem.*, **12**, 103 (1999).
[2] E.M.F. Muri, M.J. Nieto, R.D. Sindelar, J.S. Williamson. *Curr. Med. Chem.*, **9**, 1631 (2002).
[3] L. Huanting, Y. Gong, Q. Zhong. *Curr. Top. Med. Chem.*, **21**, 1737 (2021).
[4] M.A. Alam. *Curr. Org. Chem.*, **23**, 978 (2019).

[5] S.H. Sumrra, S. Ramzan, G. Mustafa, M. Ibrahim, E.U. Mughal, M.A. Nadeem, Z.H. Chohan, M. Khalid. *Russ. J. Gen. Chem.*, **88**, 1707 (2018).
[6] S. Khalid, S.H. Sumrra. *Z.H. Sains Malaysiana*, **49**, 1889 (2020).
[7] B.L. Gonçalves, D.F. Ramos, P.C.B. Halicki, P.E.A. da Silva, J. d M. Vicenti. *Chem. Data Collect.*, **22**, 1 (2019).
[8] K. Devendra, T. Rashmi. *J. Inst. Chem.*, **82**, 21 (2010).
[9] B. Shankar, R. Tomar, R. Kumar, M. Godhara, V.K. Sharma. *J. Chem. Pharm. Res.*, **6**, 925 (2014).
[10] D.A. Brown, A.L. Roche. *Inorg. Chem.*, **22**, 2199 (1983).
[11] H.D. Aliyu, J.N. Nwabueze. *Asian J. Chem.*, **23**, 34 (2011).
[12] M.J. Rao, B. Sethuram, T.N. Rao. *J. Inorg. Biochem.*, **24**, 155 (1985).
[13] M.J. Haron, H. Jahangirian, M.H.S. Ismail, R. Rafiee-Moghaddam, M. Rezayi, B. Mahdavi. *Asian J. Chem.*, **25**, 4183 (2013).
[14] T.S. Coelho, P.C.B. Halicki, L. Silva, J.R. de Menezes Vicenti, B.L. Gonçalves, P.E. Almeida da Silva, D.F. Ramos. *Lett. Appl. Microbiol.*, **71**, 146 (2020).
[15] P. Gebhardt, A.L. Crumbliss, M.J. Miller, U. Möllmann. *Biometals*, **21**, 41 (2008).
[16] X. Li, M. Xie, C. Lu, J. Mao, Y. Cao, Y. Yang, Y. Wei, X. Liu, S. Cao, Y. Song, J. Peng, Y. Zhou, Q. Jiang, G. Lin, S. Qin, M. Qi, M. Hou, X. Liu, H. Zhou, G. Yang, C. Yang. *Eur. J. Med. Chem.*, **203**, 112614 (2020).
[17] R. Mamidala, S.R.S. Bhimathati, A. Vema. *Bioorg. Chem.*, **114**, 105010 (2021).
[18] S. Sjøli, E. Nuti, C. Camodeca, I. Bilto, A. Rossello, J.O. Winberg, I. Sylte, O.A. Adekoya. *Eur. J. Med. Chem.*, **108**, 141 (2016).
[19] N.B. Vinh, N. Drinkwater, T.R. Malcolm, M. Kassiou, L. Lucantoni, P.M. Grin, G.S. Butler, S. Duffy, C.M. Overall, V.M. Avery, P.J. Scammells, S. McGowan. *J. Med. Chem.*, **62**, 622 (2019).
[20] M. Gao, Q. Lv, H. Zhang, G. Tu. *Med. Chem.*, **17**, 658 (2021).
[21] J. Choi, T. Neupane, R. Baral, J.G. Jee. *Antioxidants*, **11**, 280 (2022).
[22] G.B. Fields. *Cells*, **8**, 984 (2019).
[23] Z. Jiang, Q. You, X. Zhang. *Eur. J. Med. Chem.*, **165**, 172 (2019).
[24] A. Citarella, D. Moi, L. Pinzi, D. Bonanni, G. Rastelli. *ACS Omega*, **6**, 21843 (2021).
[25] M. Umemura, J.-H. Kim, H. Aoyama, Y. Hoshino, H. Fukumura, R. Nakakaji, I. Sato, M. Ohtake, T. Akimoto, M. Narikawa, R. Tanaka, T. Fujita, U. Yokoyama, M. Taguri, S. Okumura, M. Sato, H. Eguchi, Y. Ishikawa. *J. Pharmacol. Sci.*, **134**, 203 (2017).
[26] G.A. Hope, R. Woods, G.K. Parker, A.N. Buckley, J. McLean. *Inorg. Chim. Acta*, **365**, 65 (2011).
[27] T.W. Failes, T.W. Hambley. *Aust. J. Chem.*, **53**, 879 (2000).
[28] C.C. McSweeney, S. Hutchinson, S. Harris, J.D. Glennon. *Anal. Chim. Acta*, **346**, 93 (1997).
[29] D.A. Brown, W.K. Glass, S.J.C. McGardle. *Inorg. Chim. Acta*, **80**, 13 (1983).
[30] D.A. Brown, D. McKeith (née Byrne), W.K. Glass. *Inorg. Chim. Acta*, **35**, 5 (1979).
[31] D.A. Brown, D. McKeith, W.K. Glass. *Inorg. Chim. Acta*, **35**, 57 (1979).
[32] A. Pastuszko, K. Majchrzak, M. Czyz, B. Kupcewicz, E. Budzisz. *J. Inorg. Biochem.*, **159**, 133 (2016).
[33] F. Neese. *Rev. Comput. Mol. Sci.*, **2**, 73 (2012).
[34] J.G. Brandenburg, C. Bannwarth, A. Hansen, S. Grimme. *J. Chem. Phys.*, **148**, 64104 (2018).
[35] I. Chikh Alard, J. Soubhye, G. Berger, M. Gelbcke, S. Spassov, K. Amighi, J. Goole, F. Meyer. *Polym. Chem.*, **8**, 2450 (2017).
[36] J.H. Jorgensen, J.D. Turnidge. *Man. Clin. Microbiol.*, **9**, 1152 (2007).
[37] R. Hałasa, K. Turecka, C. Orlewska, W. Werel. *J. Microbiol. Methods*, **107**, 98 (2014).
[38] K. Konaté, J.F. Mavoungou, A.N. Lepengué, R.R.R. Aworet-Samseny, A. Hilou, A. Souza, M.H. Dicko, B. M'Batchi. *Ann. Clin. Microbiol. Antimicrob.*,**11**, 18 (2012).
[39] T. Mosmann. *J. Immunol. Methods*, **65**, 55 (1983).
[40] L. Rafols, D. Josa, D. Aguilà, L.A. Barrios, O. Roubeau, J. Cirera, V. Soto-Cerrato, R. Pérez-Tomás, M. Martínez, A. Grabulosa, P. Gamez. *Inorg. Chem.*, **60**, 7974 (2021).
[41] L.R. Hassan, E.H. Anouar, H. Bahron, F. Abdullah, A. Mohd Tajuddin. *J. Biol. Inorg. Chem.*, **25**, 239 (2020).

[42] N. Engel, A. Falodun, J. Kühn, U. Kragl, P. Langer, B. Nebe. *BMC Complement. Altern. Med.*, **14**, 1 (2014).
[43] P.B. da Silva, B.V. Bonifácio, R.C.G. Frem, A.V. Godoy Netto, A.E. Mauro, A. M. d C. Ferreira, E. d O. Lopes, M.S.G. Raddi, T.M. Bauab, F.R. Pavan, M. Chorilli. *Molecules*, **20**, 22534 (2015).
[44] A.S. Reddy, M.S. Kumar, G.R. Reddy. *Tetrahedron Lett.*, **41**, 6285 (2000).
[45] D.A. Brown, W.K. Glass, R. Mageswaran, B. Girmay. *Magn. Reson. Chem.*, **26**, 970 (1988).
[46] E.; Bayer. *CH 440314 WO*, 1229 1967
[47] F. Zhu, J. Wu, G. Chen, W. Lu. *J. Pan. Nat. Prod. Commun.*, **6**, 1137 (2011).
[48] D.M. Griffith, B. Szocs, T. Keogh, K.Y. Suponitsky, E. Farkas, P. Buglyó, C.J. Marmion. *J. Inorg. Biochem.*, **105**, 763 (2011).
[49] L.K. Omosa, J.O. Midiwo, A.T. Mbaveng, S.B. Tankeo, J.A. Seukep, I.K. Voukeng, J.K. Dzotam, J. Isemeki, S. Derese, R.A. Omolle, T. Efferth, V. Kuete. *Springerplus*, **5**, 901 (2016).
[50] B. Chatterjee. *Coord. Chem. Rev.*, **26**, 281 (1978).
[51] S.A. Benguzzi, A.A. El-Warfalli. *Pelagia Res. Libr. Chem. Sin.*, **5**, 47 (2014).
[52] A.E. Harvey, D.L. Manning. *J. Am. Chem. Soc.*, **72**, 4488 (1950).
[53] S. Dhungana, S. Heggemann, P. Gebhardt, U. Möllmann, A.L. Crumbliss. *Inorg. Chem.*, **42**, 42 (2003).
[54] D.E. Çirali, Z. Uyar, I. Koyuncu, N. Hacio¡lu. *Appl. Organomet. Chem.*, **29**, 536 (2015).
[55] L.R. Hassan, E.H. Anouar, H. Bahron, F. Abdullah, A. Mohd Tajuddin. *J. Biol. Inorg. Chem.*, **25**, 239 (2020).
[56] V.K. Jindal, M.C. Agrawal, S.P. Mushran. *J. Chem. Soc. A*, 2060 (1970).
[57] S. Ozaki, M. Masui. *Chem. Pharm. Bull.*, **25**, 1179 (1977).
[58] J.E. Rowe, A.D. Ward. *Aust. J. Chem.*, **21**, 2761 (1968).
[59] A. Samuni, S. Goldstein. *J. Phys. Chem. A*, **115**, 3022 (2011).
[60] U. Samuni, E. Maimon, S. Goldstein. *J. Coord. Chem.*, **71**, 1728 (2018).
[61] O. Onomura. In *PATAI'S Chem. Funct. Groups*, Z. Rappoport (Ed), Wiley, Hoboken (2008).
[62] A.K.C. Mengel, C. Förster, A. Breivogel, K. Mack, J.R. Ochsmann, F. Laquai, V. Ksenofontov, K. Heinze. *Chemistry*, **21**, 704 (2015).
[63] F.P.L. Andrieux, C. Boxall, H.M. Steele, R.J. Taylor. *J. Solution Chem.*, **43**, 608 (2014).
[64] K.K. Ghosh. *Indian J. Chem. Sect. B: Org. Med. Chem.*, **36**, 1089 (1997).
[65] H. Irving, R.J.P. Williams. *Nature*, **162**, 746 (1948).
[66] K.H. Scheller, T.H. Abel, P.E. Polanyi, P.K. Wenk, B.E. Fischer, H. Sigel. *Eur. J. Biochem.*, **107**, 455 (1980).
[67] D.R. Lide. *Handbook of Chemistry and Physics*, **86**, 4 (2006).
[68] H.H. Bayoumi, A.N. Alaghaz, M.S. Aljahdali. *Int. J. Electrochem. Sci.*, **8**, 9399 (2013).
[69] S. Chandra, N. Gupta, R. Gupta, S.S. Bawa. *Spectrochim. Acta A Mol. Biomol. Spectrosc.*, **62**, 552 (2005).
[70] S.H. Sumrra, W. Zafar, H. Javed, M. Zafar, M.Z. Hussain, M. Imran, M.A. Nadeem. *Biometals*, **34**, 1329 (2021).
[71] S. Rani, S.H. Sumrra, Z.H. Chohan. *Russ. J. Gen. Chem.*, **87**, 1834 (2017).
[72] N. Raman, A. Kulandaisamy, C. Thangaraja, P. Manisankar, S. Viswanathan, C. Vedhi. *Transit. Met. Chem.*, **29**, 129 (2004).
[73] S. Celen, E. Gungor, H. Kara, A.D. Azaz. *J. Coord. Chem.*, **66**, 3170 (2013).
[74] S. Chandraleka, K. Ramya, G. Chandramohan, D. Dhanasekaran, A. Priyadharshini, A. Panneerselvam. *J. Saudi Chem. Soc.*, **18**, 953 (2014).
[75] H. Maehr. *Pure Appl. Chem.*, **28**, 603 (1971).
[76] J. Hase, K. Kobashi, N. Kawaguchi, K. Sakamoto. *Chem. Pharm. Bull. (Tokyo)*, **19**, 363 (1971).
[77] S. Ammendola, A. Lembo, A. Battistoni, P. Tagliatesta, C. Ghisalberti, A. Desideri. *FEMS Microbiol. Lett.*, **294**, 61 (2009).
[78] L. Brown, J.M. Wolf, R. Prados-Rosales, A. Casadevall. *Nat. Rev. Microbiol.*, **13**, 620 (2015).
[79] T.J. Silhavy, D. Kahne, S. Walker. *Perspect. Biol.*, **2**, 1 (2010).
[80] S.A.A. Jamal, B. Jaser, W.F. Hmadi, O. Al Obaidi. *Syst. Rev. Pharm.*, **11**, 109 (2020).

[81] W.H. Mahmoud, G.G. Mohamed, M.M.I. El-Dessouky. *Spectrochim. Acta A Mol. Biomol. Spectrosc.*, **122**, 598 (2014).
[82] N. Dharmaraj, P. Viswanathamurthi, K. Natarajan. *Transit. Met. Chem.*, **26**, 105 (2001).
[83] Y. Samuni, U. Samuni, S. Goldstein. *Biochim. Biophys. Acta*, **1820**, 1560 (2012).
[84] R. Ortmann, J. Wiesner, K. Silber, G. Klebe, H. Jomaa, M. Schlitzer. *Arch. Pharm. (Weinheim)*, **340**, 483 (2007).
[85] C. Bisignano, F.A. Franchina, P.Q. Tranchida, L. Mondello, G. Mandalari. *Molecules*, **24**, 1276 (2019).
[86] W. Liu, Y. Qin, S. Liu, R. Xing, H. Yu, X. Chen, K. Li, P. Li. *Int. J. Biol. Macromol.*, **106**, 68 (2018).
[87] Y. Liu, L. He, A. Mustapha, H. Li, Z.Q. Hu, M. Lin. *J. Appl. Microbiol.*, **107**, 1193 (2009).
[88] J.Y. Lee, M.C. Jeong, D. Jeon, Y. Lee, W.C. Lee, Y. Kim. *Bioorg. Med. Chem.*, **25**, 372 (2017).
[89] T. Simonart, J.C. Noel, Y. Lunardi-Yskandar. *Int. J. Cancer*, **78**, 720 (1998).
[90] R. Pakdaman, F.B. Abdallah, J.M. El Hage Chahine. *J. Mol. Biol.*, **293**, 1273 (1999).
[91] B.G. Tweedy. *Phytopathology*, **55**, 910 (1964).